Notes

Contents

1 Introduction

1.1 Metaphysical introduction

The currently established theory of gravity is based on the idea that "curved spacetime tells matter how to move" and that "matter tells spacetime how to curve". In fact, the device of spacetime has been so successful that it has already been built into the languages we speak. However, it is not always realized how abstract the information is that theoretical physics gives. Ordinary language is unsuited for expressing what physics tries to assert. Even more, all that physics gives us are certain functional equations that allow us to organize and structure events *we* experience. Physics is silent about whether our notions appearing in the equations (like electrical fields, spacetime or entangled spinor quantum fields) represent an underlying "physical reality". In fact, it would be a mistake to introduce our abstract concepts into the world and reify them. In Niels Bohr's words: "It is wrong to think that the task of physics is to find out how nature is. Physics concerns what we can say about nature." *Understanding theories about the world* is a much lower aspiration that *understanding the world*. One could go further and even assert that "*my* physics concern what *I* can say about *my* world." Such positions may be purely motivated by philosophy, but thinking about quantum mechanics has also brought such positions to some physicists.

In this light, what do I mean when I say "space-time", a word which lies at the foundations of the theory of general relativity? What *is* spacetime? In light of the above position I would answer: Time and space are modes by which I think, which I invented to organize events I experience; space and time are not conditions in which I live (apparently this quote is even attributed to Einstein, but this seems unlikely since the content is hard to reconcile with his objections to quantum mechanics.) In any case, in this chapter I give a frightening abstract definition of a manifold. The abstractness of this first section is intended to remind myself that I should refrain from reifing mathematical or mental concepts into the world. What does it possibly mean that a locally ringed space locally isomorphic to $(\mathbb{R}^4, \mathcal{C}^\infty_{\mathbb{R}^4})$ with its sheaf of differentiable functions "is really out there"? When one adopts Bourbaki's philosophy that everything in mathematics can be accommodated within set theory, the "ontology of spacetime" is reduced to the "ontology of set theory". So, what meaning has the question: Is set theory "out there"?

In physics coordinates systems are used all the time. At the same time, especially in general relativity, it is acknowledged that local coordinates have no prominent role in the theory. Nevertheless, the usual construction of "space-time", that is of manifolds with some extra structure, explicitly uses local coordinate charts; this can lead to overemphasize them and to conceptual confusion as well. A second purpose of this section is to provide an antidote to this by outlining a construction of "space-time" where charts and atlases do not play any central role whatsoever. However, it has to be admitted that this is a purely foundational issue and the adopted viewpoint is not much of a practical use in general relativity and even differential geometry.

1.2 Mathematical introduction

One key insight of algebraic geometry is that we can understand spaces by understanding the functions on them; more precisely, we can understand a space by characterizing all functions on all open subsets of this space. This kind of information is encoded in the sheaf of functions on a space. In this light, we can define basic geometric models by their sheaves. We can then built richer geometries by gluing together these basic objects in a way that is made precise by the notion of ringed spaces and morphisms between them. This framework is indispensable for algebraic geometry, but it can also be used to give a very concise formulation of a manifold. A reference for everything in this section is *e.g.* the Stacks Project [1].

1.2.1 Sheaves

Roughly speaking, a presheaf is a way to assign data locally to open subsets of a topological space in such a way that it is compatible with restrictions. A sheaf is a presheaf for which it is possible to reassemble global information about a space from local data.

Presheaves A presheaf of $\mathcal{C}$ on a topological space X is a contravariant functor $\mathcal{F} : \mathrm{Ouv}(X) \longrightarrow \mathcal{C}$. The category $\mathrm{Ouv}(X)$ is the category whose objects are the open subsets of X and whose morphisms are inclusions. Usually $\mathcal{C}$ is the category of sets, rings, groups, ... The elements in $\mathcal{F}(U)$ are called the sections of $\mathcal{F}$ over U. Given $V \subseteq U$ in $\mathrm{Ouv}(X)$ and the inclusion map $f : V \to U$, the map $\mathcal{F}(f) : \mathcal{F}(U) \longrightarrow \mathcal{F}(V)$ is denoted by res_V^U and is called the restriction map.

Given a topological space X, we can map an open set U to the set of smooth maps $U \longrightarrow \mathbb{R}$. The set $C^\infty(U, \mathbb{R})$ has the structure of a ring, therefore we have a presheaf $\mathcal{C}_X^\infty$ of rings on X ("presheaf of smooth functions on X"). The restriction map restricts a smooth map $U \longrightarrow \mathbb{R}$ to the open subspace $V \subseteq U$.

Sheaves A presheaf $\mathcal{F}$ is a sheaf if given any open subset $U \subset X$ and an open cover $U = \bigcup_\alpha U_\alpha$, the two conditions are satisfied

1. if $s, t \in \mathcal{F}(U)$ are such that $s|_{U_\alpha} = t|_{U_\alpha}$ for all α, then $s = t$ in $\mathcal{F}(U)$,

2. if $s_\alpha \in \mathcal{F}(U_\alpha)$ is a collection of sections which agree when restricted to their intersections $U_\alpha \cap U_\beta$, then there is a $s \in \mathcal{F}(U)$ which restricts to each s_α on $U_\alpha \subseteq U$.

The presheaf of smooth functions is a sheaf. Indeed, in a somewhat obvious way we have:

1. Let $s, t : U \to \mathbb{R}$ and suppose that s and t agree on each open subset in a cover of U. We need to show that $s(x) = t(x)$ for all $x \in U$. Let $x \in U$, then $u \in U_i$ for some i. We then have $s(x) = s|_{U_i}(x) = t|_{U_i}(x) = t(x)$.

2. Let $U = \bigcup_i U_i$ and let s_i be sections which agree on their intersections. We can define a map $s : U \to \mathbb{R}$ by taking $x \in U$ and some U_i which contains x, and setting $s(x) = s_i(x)$. This is independent of the U_i chosen, because all s_i agree on intersections. The function s is smooth since all s_i are smooth and since smoothness of a function is a local property.

Let $\mathcal{F}$ and $\mathcal{G}$ be presheaves of $\mathcal{C}$ on X. A morphism of presheaves $\phi : \mathcal{F} \to \mathcal{G}$ is a family of morphisms in $\mathcal{C}$ $\phi_U : \mathcal{F}(U) \to \mathcal{G}(U)$ for each open $U \subset X$ such that given an inclusion $V \subseteq U$ we have the commutative diagram

$$
\begin{array}{ccc}
\mathcal{F}(U) & \xrightarrow{\ \phi_U\ } & \mathcal{G}(U) \\
{\scriptstyle\mathrm{res}^U_V}\downarrow & & \downarrow{\scriptstyle\mathrm{res}^U_V} \\
\mathcal{F}(V) & \xrightarrow{\ \phi_V\ } & \mathcal{G}(V).
\end{array}
$$

A morphism of sheaves is a morphism of the underlying presheaves. We also need a tool to study sheaves and presheaves locally. For any presheaf $\mathcal{F}$ and any point $x \in X$, we define the stalk $\mathcal{F}_x$ to be

$$
\mathcal{F}_x = \{(U, s) \,|\, x \in U, s \in \mathcal{F}(U)\}/\sim,
$$

where $(U, s) \sim (U', s')$ if and only if there exists $V \subset U \cap U'$ such that $s|_V = s'|_V$.

An element of the stalk $\mathcal{C}^\infty_{X,x}$ of $\mathcal{C}^\infty_X$ at x is thus a C^∞-function f whose domain contains x. A pair of such functions f, g determine the same element of the stalk if they agree in a neighbourhood of x. Such an equivalence class is called a germ of a C^∞-function at x and the stalk $\mathcal{C}^\infty_{X,x}$ is then the ring of germs of smooth functions at x. The stalk $\mathcal{C}^\infty_{X,x}$ is a local ring with maximal ideal $\mathfrak{m} = \{[(U, f)] \,|\, f(x) = 0\}$. In other words, the ideal $\mathfrak{m}$ is the set of non-invertible elements in $\mathcal{C}^\infty_{X,x}$. Indeed, for the germ at x of a smooth function to be invertible in $\mathcal{C}^\infty_{X,x}$, it is necessary and sufficient that $f(x) \neq 0$, for this implies that $f(x) \neq 0$ in a neighbourhood of x.

Given a continuous map $f : X \to Y$ of topological spaces and a presheaf $\mathcal{F}$ on X, the pushforward $f_*\mathcal{F}$ is the presheaf on Y defined by $(f_*\mathcal{F})(V) = \mathcal{F}(f^{-1}(V))$ for $V \in \mathrm{Ouv}(Y)$. The pushforward $f_*\mathcal{F}$ of a sheaf $\mathcal{F}$ on X is a sheaf on Y.

1.2.2 Locally-ringed spaces

We will define a type of structure that lends itself well to construct spaces by gluing together different spaces along open sets.

A ringed space is a pair $(X, \mathcal{O}_X)$ consisting of a topological space and a sheaf of rings $\mathcal{O}_X$. A morphism of ringed spaces $(f, f^\sharp) : (X, \mathcal{O}_X) \to (Y, \mathcal{O}_Y)$ is a continuous map of topological spaces $f : X \to Y$ and a morphism of sheaves $f^\sharp : \mathcal{O}_Y \to f_*\mathcal{O}_X$. The map $f^\sharp$ is simply precomposition when working with ringed spaces whose sheaf is that of smooth functions. That is, to $f : X \to Y$ and $\varphi : V \to \mathbb{R} \in \mathcal{C}^\infty_Y$ there is associated the map $f^\sharp = \varphi \circ (f|_{f^{-1}(V)}) \in \mathcal{C}^\infty_X(f^{-1}(V))$.

We will impose a condition relating the geometry of X with the algebra of $\mathcal{O}_X$. One motivation for doing this really comes from algebraic geometry: The functor from the category of rings to the category of ringed spaces is not fully faithful: It is possible that there are maps between ringed spaces that are not induced by maps of rings. We therefore want to impose a condition restricting the set of morphisms. We will see that ringed spaces with sheaves of differentiable functions naturally fall into this framework.

A locally-ringed space is a ringed space $(X, \mathcal{O}_X)$ so that for all $x \in X$ the stalk $\mathcal{O}_{X,x}$ is a local ring. A morphism of locally-ringed spaces $(f, f^\sharp) : (X, \mathcal{O}_X) \to (Y, \mathcal{O}_Y)$ is a morphism of ringed spaces such that for all $x \in X$ the map of local rings $f_x^\sharp : \mathcal{O}_{Y,f(x)} \to \mathcal{O}_{X,x}$ is a local ring morphism. A morphism of local rings $f : R \to S$ is called local if $f^{-1}(\mathfrak{m}_S) = \mathfrak{m}_R$.

We already know that the stalk $\mathcal{C}_{X,x}^\infty$ is a local ring, therefore the pair $(X, \mathcal{C}_X^\infty)$ is a locally-ringed space. Given two such pairs $(X, \mathcal{C}_X^\infty)$ and $(Y, \mathcal{C}_Y^\infty)$, the map on stalks $f^\sharp : \mathcal{C}_{Y,f(x)}^\infty \to \mathcal{C}_{X,x}^\infty$ maps the maximal ideal into the maximal ideal.

One can use the established formalism to construct spaces by gluing together local patches. Here we only apply this general machinery to make the following definition:

A smooth manifold is a locally-ringed space $(X, \mathcal{O}_X)$ which admits a covering $X = \bigcup_i U_i$ by open subsets such that each $(U_i, \mathcal{O}_{X|_{U_i}})$ is isomorphic as a locally ringed space to $\{(Y, \mathcal{C}_Y^\infty) \mid Y \in \mathrm{Ouv}(\mathbb{R}^n)\}$.

A morphism of manifolds is then simply a morphism of locally-ringed spaces. Usually the definition of a smooth manifold also requires X to be Hausdorff and paracompact.

1.3 Physical introduction

1.4 Keplerian orbit parameters

Unless otherwise stated, we use throughout the text the geometrized unit system, *i.e.* we set $c = G = 1$.

Throughout the text, we often consider masses orbiting in a Keplerian orbit. We denote by $m_1 \geq m_2$ the masses of the two bodies, by $M = m_1 + m_2$ their total mass, by $q = \frac{m_2}{m_1}$ the secondary-to-primary mass ratio and by $\eta = \frac{m_1 m_2}{M^2}$ the symmetric mass ratio. We will throughout the text treat binary problems in the center-of-mass frame. In the center-of-mass-frame the two-body problem reduces to a one-body problem for a particle of reduced mass $\mu = M\eta = M\frac{q}{(1+q)^2}$ orbiting around the total mass M. The mean angular frequency (radians per unit time) is from Kepler's third law

$$\Omega = \sqrt{\frac{M}{a^3}} = \left(\frac{M(1-e)^3}{r_p^3} \right)^{1/2}, \tag{1}$$

where r_p is the orbit's pericenter distance, a the orbit's semi-major axis and e the orbit's eccentricity. The orbital period is accordingly $T = \frac{2\pi}{\Omega}$. If we set up polar coordinates (r, ϕ) in the plane of the orbit, the orbit equation for any Keplerian orbit reads

$$r = \frac{a(1-e^2)}{1 + e\cos\phi}. \tag{2}$$

1.4.1 Hyperbolic Keplerian orbits

We use the convention that for an hyperbolic orbit the semi-major axis a is negative. The semi-minor axis b of an hyperbola is also the distance from one of the foci of the hyperbola to an asymptote, therefore the semi-minor axis is also called the impact parameter. The following relations characterize an hyperbolic trajectory

$$b = -a(e^2 - 1)^{1/2} \tag{3}$$

$$= \frac{\mu M}{2E}(e^2 - 1)^{1/2} \tag{4}$$

$$= \frac{M}{v^2}(e^2 - 1)^{1/2} \tag{5}$$

$$= \frac{L}{(2E\mu)^{1/2}}. \tag{6}$$

Here v is the relative velocity of the two bodies at infinity and $L = b\mu v$ is the angular momentum. The pericenter distance is therefore

$$r_p = a(1-e) = \frac{M}{v^2}\left[\left(1 + \frac{b^2 v^4}{M^2} \right)^{1/2} - 1 \right]. \tag{7}$$

For small relative velocities v this simplifies to

$$r_p \simeq \frac{b^2 v^2}{2M}\left(1 - \frac{b^2 v^4}{4M^3} \right). \tag{8}$$

1.4.2 Elliptic Keplerian orbit

The eccentricity of an ellipse is defined through the semiaxes as

$$e^2 = 1 - \frac{b^2}{a^2}. \tag{9}$$

The orbital energy of two bodies on an elliptic Keplerian orbit is inversely proportional to the semi-major axis

$$E = -\frac{\eta M^2}{2a}. \tag{10}$$

The absolute value of the orbital angular momentum is

$$L = \mu\sqrt{Ma(1 - e^2)} = \mu\Omega a^2 \sqrt{1 - e^2}. \tag{11}$$

We can then write for the eccentricity

$$e^2 = 1 + \frac{2EL^2}{M^2 \mu^3}. \tag{12}$$

1.4.3 Evolution equations of e and a

The evolution equations of the eccentricity and semi-major axis of a bound binary are obtained by differentiating equations (10) and (12). We obtain

$$\frac{d\log a}{dt} = \frac{1}{a}\frac{da}{dt} = -\frac{\dot{E}}{E} + \frac{2\dot{M}}{M} + \frac{\dot{\eta}}{\eta}, \tag{13}$$

and

$$\frac{de}{dt} = \frac{1 - e^2}{2e}\left[-\frac{2\dot{L}}{L} - \frac{\dot{E}}{E} + \frac{2\dot{M}}{M} - \frac{3\dot{\mu}}{\mu}\right]. \tag{14}$$

Under the assumption that $\dot{M} = \dot{\mu} = 0$, the last equation can be rewritten as

$$\frac{de}{dt} = \frac{a(1 - e^2)}{e\mu M}\left[\dot{E} - \frac{M^{1/2}}{a^{3/2}(1 - e^2)^{1/2}}\dot{L}\right]. \tag{15}$$

Thus $\dot{E} < 0$ is a negative contribution to $\dot{e}$ and $\dot{L} < 0$ is a positive contribution to $\dot{e}$.

2 Aspects of gravitational wave emission

In this section we briefly describe the multipole decomposition formalism in linearised general relativity as given by Thorne [2]. Then this formalism is applied to determine in the mass quadrupole approximation the energy loss, angular momentum loss and energy spectrum for binary systems on elliptic and hyperbolic Keplerian orbits.

2.1 Multipole expansion formalism

In the wave zone, gravitational waves can be treated as linearised perturbations propagating on a flat background metric. This background metric can be characterized by a Minkowskiian coordinate system whose origin coincides with the source. In this coordinate frame the transverse and traceless part of the metric perturbation has then the form

$$h_{ij}^{TT} = \frac{1}{r} A_{ij}(t - r, \theta, \phi), \tag{16}$$

where A_{ij} is a traceless and transverse tensor varying in the wave zone rapidly in the radial direction but slowly in the transverse direction. The angular dependence of the radiation field A_{ij} can be decomposed into spherical harmonics. The most suitable set are the pure-spin harmonics with well-defined transversality and helicity properties. Because A_{ij} is traceless and transverse, it contains only the transverse and traceless harmonics $\mathbf{T}^{\mathrm{E2},lm}$ and $\mathbf{T}^{\mathrm{B2},lm}$. The purely longitudinal, purely transversal or mixed longitudinal and transversal components are not encountered in standard general relativity, but need to be included in other metric theories of gravity. For $l = 0$ and $l = 1$ there are no transverse traceless harmonics. Therefore the general form of radiation field has the form

$$h_{ij}^{TT} = \frac{1}{r} \sum_{l=2}^{\infty} \sum_{m=-l}^{l} \left[{}^{(l)}I^{lm}(t - r) \, T_{ij}^{\mathrm{E2},lm} + {}^{(l)}S^{lm}(t - r) \, T_{ij}^{\mathrm{B2},lm} \right]. \tag{17}$$

The expansion coefficients ${}^{(l)}I^{lm}$ and ${}^{(l)}S^{lm}$ are the l-th time derivative of I^{lm} and S^{lm}. The components I^{lm} and S^{lm} are said to be responsible for mass multipole radiation and current multipole radiation respectively. For that reason, the leading order terms I^{2m} are responsible for the mass quadrupole radiation, terms associated with S^{2m} are called current quadrupole contributions, terms arising from I^{3m} are called mass octupole contributions, etc.
The explicit expression of I^{lm} is given by

$$I^{lm} = \frac{16\pi}{(2l + 1)!!} \left(\frac{(l + 1)(l + 2)}{2l(l - 1)} \right)^{1/2} \mathcal{G}_{A_l} \mathcal{Y}_{A_l}^{lm*}, \tag{18}$$

with the mass multipole moments $\mathcal{G}_{A_l}$. The general form of the mass multipole moments $\mathcal{G}_{A_l}$ is given by a sum of several integrals involving the energy-stress tensor and spherical Bessel functions, see equation (5.9a) in [2]. Our calculations will only involve the second mass moments, for which $\mathcal{G}_{A_2}$ in the Newtonian limit becomes equation (23). We also don't need expressions for the current multipole contributions S^{lm} in this work.

8

In the next section we will make use of the following STF tensors

$$\mathcal{Y}^{22} = \left(\frac{15}{32\pi}\right)^{1/2} \begin{pmatrix} 1 & i & 0 \\ i & -1 & 0 \\ 0 & 0 & 0 \end{pmatrix},$$ (19)

$$\mathcal{Y}^{21} = -\left(\frac{15}{32\pi}\right)^{1/2} \begin{pmatrix} 0 & 0 & 1 \\ 0 & 0 & i \\ 1 & i & 0 \end{pmatrix},$$ (20)

$$\mathcal{Y}^{20} = \left(\frac{5}{16\pi}\right)^{1/2} \begin{pmatrix} -1 & 0 & 0 \\ 0 & -1 & 0 \\ 0 & 0 & 2 \end{pmatrix},$$ (21)

together with $\mathcal{Y}^{2-m} = (-1)^m \left(\mathcal{Y}^{2m}\right)^*$.

2.1.1 Energy loss

In the multipole formalism the total radiated power is given by

$$P = \frac{dE}{dt} = \frac{1}{32\pi} \sum_{l=2}^{\infty} \sum_{m=-l}^{l} \left\langle |^{(l+1)}I^{lm}|^2 + |^{(l+1)}S^{lm}|^2 \right\rangle.$$ (22)

In case of a periodic motion, the brackets denote orbital averaging of the expression. In case of unbound motion, the brackets are to be understood as the integral of the expression over the entire orbit. In what follows, we only consider mass quadrupole radiation, that is, we consider only contributions arising from I^{2m}. If the source is non-relativistic and has a negligible self-gravity, it is possible to express the second mass moment $\mathcal{G}_{a_1 a_2}$ in terms of the Newtonian mass density ρ

$$\mathcal{G}_{a_1 a_2} = \int d^3x \, \rho \, x_{a_1} x_{a_2}.$$ (23)

Then

$$I^{2m} = \frac{16\pi}{5\sqrt{3}} \int d^3x \, \rho \, \mathcal{Y}^{2m*}_{a_1 a_2} \, x_{a_1} x_{a_2}$$ (24)

$$\equiv \frac{16\pi}{5\sqrt{3}} \int d^3x \, \rho \, r^2 Y^{2m*}.$$ (25)

2.1.2 Angular momentum loss

In the multipole expansion formalism, the change in angular momentum of a system due to gravitational wave emission is given by

$$\frac{dL_j}{dt} = \sum_{l=2}^{\infty} \frac{(l+1)(l+2)}{(l-1)l!(2l+1)!!} \left\langle \epsilon_{jpq} {}^{(l)}\mathcal{G}_{pA_{l-1}} {}^{(l+1)}\mathcal{G}_{qA_{l-1}} \right\rangle$$ (26)

$$+ \sum_{l=2}^{\infty} \frac{4l^2(l+2)}{(l-1)(l+1)!(2l+1)!!} \left\langle \epsilon_{jpq} {}^{(l)}\mathcal{S}_{pA_{l-1}} {}^{(l+1)}\mathcal{S}_{qA_{l-1}} \right\rangle.$$ (27)

In the mass quadrupole approximation this reduces to

$$\frac{dL_j}{dt} = \frac{2}{5} \left\langle \epsilon_{jpq} {}^{(2)}\mathcal{G}_{pa} {}^{(3)}\mathcal{G}_{qa} \right\rangle.$$ (28)

2.2 Application to binaries on Keplerian orbits

In this section we calculate, for binaries on a Keplerian orbit and for all $e \geqslant 0$, the energy flux, angular momentum flux and energy spectrum resulting from gravitational wave emission in the mass quadrupole approximation.

The energy emitted by gravitational waves from an elliptic Keplerian binary system was first calculated by Peters & Mathews [3]. The first calculation of the angular momentum loss for elliptic orbits is due to Peters [4]. The analogous expressions for binary systems on hyperbolic orbits were first derived by Hansen [5], both contain minor numerical mistakes. The error in Hansen's expression for the energy flux was rectified by Turner [6] and the first correct expression for the angular momentum flux is found in Junker & Schäfer [7]. The first determination of the elliptic frequency spectrum is given in Peters and Mathews's paper. A first complete calculation of the hyperbolic frequency spectrum is found in DeVittori *et al.* [8], their computation was subsequently corrected by García-Bellido & Nesseris [9]. In subsection (2.2.3) we will fix a minor inaccuracy that is present throughout [8] and [9].

2.2.1 Energy loss

We choose a coordinate system whose origin coincides with the center of mass of the system and we let the binary lie in the $\theta = \pi/2$-plane. The two masses can then be specified by $(r_1 \cos \phi, r_1 \sin \phi)$ and $(-r_2 \cos \phi, -r_2 \sin \phi)$ with $r_i = \frac{\mu r}{m_i}$. We obtain using equation (25)

$$I^{2m} = \frac{16\pi}{5\sqrt{3}} \left[m_1 \frac{\mu^2 r^2}{m_1^2} Y^{2m*} \left(\frac{\pi}{2}, \phi \right) + m_2 \frac{\mu^2 r^2}{m_2^2} Y^{2m*} \left(\frac{\pi}{2}, \phi + \pi \right) \right]. \qquad (29)$$

Because the $Y^{2\pm1*} \left(\frac{\pi}{2}, \phi \right)$ terms vanish, it is possible to set in the above expression $Y^{2m*} \left(\frac{\pi}{2}, \phi \right)$ equal to $Y^{2m*} \left(\frac{\pi}{2}, \phi + \pi \right)$. Hence we can write

$$I^{2m} = \frac{16\pi}{5\sqrt{3}} \mu r^2 Y^{2m*} \left(\frac{\pi}{2}, \phi \right). \qquad (30)$$

In the quadrupole approximation the power radiated by the system reduces from expression (22) to

$$P = \frac{1}{32\pi} \sum_{m=-2}^{2} |{}^{(3)}I^{2m}|^2. \qquad (31)$$

The orbit equations

$$r = \frac{r_p(1 + e)}{1 + e \cos \phi},$$
$$r^2 \frac{d\phi}{dt} = [M r_p (1 + e)]^{1/2}. \qquad (32)$$

allow the calculation of the time derivatives of I^{2m}. Employing these identities and using the explicit expression of the spherical harmonics Y^{2m*}, the third

time derivatives of I^{2m} read

$$^{(3)}I^{20} = \left(\frac{64\pi}{15}\right)^{1/2} \frac{\mu M^{3/2}}{[r_p(1+e)]^{5/2}} (1+e\cos\phi)^2 e\sin\phi,$$

$$^{(3)}I^{2-2} = \left(\frac{32\pi}{5}\right)^{1/2} \frac{\mu M^{3/2}}{[r_p(1+e)]^{5/2}} (1+e\cos\phi)^2 \left[-e\sin\phi - 4i(1+e\cos\phi)\right]e^{2i\phi},$$

$$^{(3)}I^{22} = \left(^{(3)}I^{2-2}\right)^*.$$

The radiated power as a function of ϕ along the orbit is then

$$P(\phi) = \frac{8}{15}\frac{\mu^2 M^3}{[r_p(1+e)]^5} (1+e\cos\phi)^4 \left[e^2\sin^2\phi + 12(1+e\cos\phi)^2\right]. \qquad (33)$$

Note that this expression is valid for all values of $e \geq 0$.

Hyperbolic orbit $e \geq 1$: The asymptotes of an hyperbolic orbit are given by $\cos\psi = -1/e$. Thus the total energy released by a binary on an hyperbolic orbit is

$$E = \int_{-\psi}^{\psi} P(\phi)\frac{dt}{d\phi}\,d\phi \qquad (34)$$

$$= \frac{8}{15}\frac{\eta^2 M^{9/2}}{(r(1+e))^{7/2}} \int_{-\psi}^{\psi} d\phi\,(1+e\cos\phi)^2 \left[e^2\sin^2\phi + 12(1+e\cos\phi)^2\right] \qquad (35)$$

$$= \frac{\eta^2 M^{9/2}}{r_p^{7/2}(1+e)^{7/2}}\varrho(e), \qquad (36)$$

where

$$\varrho(e) = \frac{1}{180}\left[(12(96 + 292e^2 + 37e^4)\phi + 48e(96 + 73e^2)\sin\phi\right.$$

$$\left. + 24e^2(71 + 12e^2)\sin 2\phi + 368e^3\sin 3\phi + 33e^4\sin 4\phi\right]_{-\psi}^{\psi}$$

$$= \frac{64}{5}\left[\left(1 + \frac{73}{24}e^2 + \frac{37}{96}e^4\right)\cos^{-1}\left(-\frac{1}{e}\right) + \frac{301}{144}(e^2-1)^{1/2}\left(1 + \frac{673}{602}e^2\right)\right].$$

For a parabolic orbit, $e = 1$, the radiated energy becomes

$$E = \frac{85\pi}{12\sqrt{2}}\frac{\eta^2 M^{9/2}}{r_p^{7/2}}. \qquad (37)$$

Elliptic orbit $e < 1$: In case of elliptic orbits, the average of $P(\phi)$ over one orbital period gives

$$\frac{dE}{dt} = P = \frac{\Omega}{2\pi}\int_0^{2\pi} P(\phi)\frac{dt}{d\phi}\,d\phi$$

$$= \frac{8}{15}\frac{1}{(1-e^2)^{7/2}}\frac{\mu^2 M^3}{a^5}\int_0^{2\pi}\frac{d\phi}{2\pi}(1+e\cos\phi)^2\left[e^2\sin^2\phi + 12(1+e\cos\phi)^2\right].$$

After performing the integral we arrive at

$$\frac{dE}{dt} = \frac{32}{5}\frac{\mu^2 M^3}{a^5}\frac{1}{(1-e^2)^{7/2}}\left(1 + \frac{73}{24}e^2 + \frac{37}{96}e^4\right). \qquad (38)$$

11

There is a simple way to deduce the energy loss of a parabolic orbit from the energy loss of an elliptic orbit. The energy radiated per orbit is $E = \frac{2\pi}{\Omega}P$. For a parabolic orbit, the energy radiated per orbit is the total energy radiated. By analytically continuing the orbital parameters to $e = 1$, we then obtain indeed equation (37). An extension of the results from $e < 1$ beyond $e = 1$ is, when resorting to the parametrization used here, not possible.

2.2.2 Angular momentum loss

We now proceed to determine the GW-induced angular momentum loss of a binary on a Keplerian orbit. To this end we choose a coordinate system such that the orbits lies in the (x, y)−plane; then we can set $L = L_z$. Therefore we have

$$\frac{dL}{dt} = \frac{2}{5}\left({}^{(2)}\mathcal{G}_{1a}{}^{(3)}\mathcal{G}_{2a} - {}^{(2)}\mathcal{G}_{2a}{}^{(3)}\mathcal{G}_{1a} \right). \tag{39}$$

The second mass moments in our chosen coordinate frame are given by

$$\mathcal{G} = \mu r^2 \begin{bmatrix} \cos^2\phi & \cos\phi\sin\phi & 0 \\ \cos\phi\sin\phi & \sin^2\phi & 0 \\ 0 & 0 & 0 \end{bmatrix}. \tag{40}$$

By making use of the orbit equations (32), we can calculate the required derivatives and obtain

$${}^{(2)}\mathcal{G}_{12} = -\frac{\mu M}{r_p(1+e)}\sin\phi\,[4\cos\phi + e(3 + \cos(2\phi))],$$

$${}^{(3)}\mathcal{G}_{12} = -\left(\frac{\mu^2 M^3}{4[r_p(1+e)]^5}\right)^{1/2}(1 + e\cos\phi)^2(5e\cos\phi + 8\cos(2\phi) + 3e\cos(3\phi)),$$

$${}^{(2)}\mathcal{G}_{11} = -\frac{\mu M}{2r_p(1+e)}(3e\cos\phi + 4\cos(2\phi) + e\cos(3\phi)),$$

$${}^{(3)}\mathcal{G}_{11} = \left(\frac{\mu^2 M^3}{[r_p(1+e)]^5}\right)^{1/2}(1 + e\cos\phi)^2(4 + 3e\cos\phi)\sin(2\phi),$$

$${}^{(2)}\mathcal{G}_{22} = \frac{\mu M}{2r_p(1+e)}[7e\cos\phi + 4\cos(2\phi) + e(4e + \cos(3\phi))],$$

$${}^{(3)}\mathcal{G}_{22} = -\left(\frac{\mu^2 M^3}{[r_p(1+e)]^5}\right)^{1/2}(1 + e\cos\phi)^2[8\cos\phi + e(5 + 3\cos(2\phi))]\sin\phi.$$

The angular momentum emitted as a function of ϕ along the orbit is then

$$\frac{dL}{dt} = \frac{4}{5}\frac{\mu^2 M^{5/2}}{[r_p(1+e)]^{7/2}}(1 + e\cos\phi)^3(8 + e^2 + 12e\cos\phi + 3e^2\cos(2\phi)). \tag{41}$$

Hyperbolic orbit $e \geq 1$: The angular momentum loss integrated over the entire hyperbolic orbit is

$$L = \int_{-\psi}^{\psi} \frac{dL}{dt} \frac{dt}{d\phi} \, d\phi \tag{42}$$

$$= \frac{4}{5} \frac{\mu^2 M^2}{[r_p(1+e)]^2} \int_{-\psi}^{\psi} d\phi \, (1 + e \cos \phi)(8 + e^2 + 12e \cos \phi + 3e^2 \cos(2\phi)) \tag{43}$$

$$= \frac{4}{5} \frac{\mu^2 M^2}{[r_p(1+e)]^2} \, \varpi|_{-\psi}^{\psi}, \tag{44}$$

where

$$\varpi = 8\phi + 7e^2\phi + 20e \sin \phi + \frac{5}{2}e^3 \sin \phi + \frac{9}{2}e^2 \sin(2\phi) + \frac{1}{2}e^3 \sin(3\phi).$$

The evaluation of ϖ between $-\psi = -\cos^{-1}(-1/e)$ and $\psi = \cos^{-1}(-1/e)$ gives

$$\varpi|_{-\psi}^{\psi} = 2\left(8 + 7e^2\right) \cos^{-1}\left(-\frac{1}{e}\right) + 2(e^2 - 1)^{1/2}\left(13 + 2e^2\right). \tag{45}$$

For a parabolic orbit, $e = 1$, the emitted angular momentum becomes

$$L = 6\pi \frac{\mu^2 M^2}{r_p^2}. \tag{46}$$

Elliptic orbit $e < 1$: In case of elliptic orbits, the angular momentum change averaged over one orbital period is

$$\frac{dL}{dt} = \frac{\Omega}{2\pi} \int_0^{2\pi} \frac{dL}{dt} \frac{dt}{d\phi} \, d\phi$$

$$= \frac{4}{10\pi} \frac{\mu^2 M^{5/2}}{r_p^{7/2}} \frac{(1-e)^{3/2}}{(1+e)^2} \, \varpi|_0^{2\pi}.$$

The expression $\varpi|_0^{2\pi}$ evaluates to $2\pi(8 + 7e^2)$ and we have

$$\frac{dL}{dt} = \frac{32}{5} \frac{\mu^2 M^{5/2}}{a^{7/2}} \frac{1}{(1-e^2)^2} \left(1 + \frac{7}{8}e^2\right). \tag{47}$$

Analogous to previous subsection, we can perform an analytical continuation of the above result to $e = 1$, thereby again obtaining the parabolic limit (46) of the hyperbolic case.

2.2.3 Frequency spectrum

In this section we compute for all $e \geq 0$ the frequency spectrum of the radiated power. The key ingredient for this is to perform a Fourier decomposition of the binary's second mass moment.

Elliptic orbit $e < 1$: We parametrize an elliptic Keplerian orbit in the following form

$$x(\beta) = a(\cos u - e), \tag{48}$$
$$y(\beta) = b \sin u. \tag{49}$$

Here a is the semi-major axis and b is the semi-minor axis of the orbit. The eccentric anomaly u is defined by the Kepler equation

$$u - e \sin u = \Omega t \equiv \beta. \tag{50}$$

The second mass moment has then the form

$$\mathcal{G} = \mu \begin{bmatrix} a^2(\cos u - e)^2 & ab(\cos u - e)\sin u & 0 \\ ab(\cos u - e)\sin u & b^2 \sin^2 u & 0 \\ 0 & 0 & 0 \end{bmatrix} \tag{51}$$

$$= \mu \begin{bmatrix} a^2(-2e\cos u + \frac{1}{2}\cos(2u) + e^2 + \frac{1}{2}) & ab(-e\sin u + \frac{1}{2}\sin(2u)) & 0 \\ ab(-e\sin u + \frac{1}{2}\sin(2u)) & \frac{b^2}{2}(1 - \cos(2u)) & 0 \\ 0 & 0 & 0 \end{bmatrix}. \tag{52}$$

The emitted power in the mass quadrupole approximation is obtained from the formulae (18) and (31)

$$P = \frac{8\pi}{75} \sum_{m=-2}^{2} \left\langle \left| {}^{(3)}\mathcal{G}_{a_1 a_2} \left(\mathcal{Y}_{a_1 a_2}^{2m} \right)^* \right|^2 \right\rangle \tag{53}$$

$$= \frac{8\pi}{75} \sum_{m=-2}^{2} \frac{1}{2T} \int_{-T}^{T} dt \left| {}^{(3)}\mathcal{G}_{a_1 a_2} \left(\mathcal{Y}_{a_1 a_2}^{2m} \right)^* \right|^2, \tag{54}$$

with the orbital period T. To find the frequency decomposition of the emitted power we can make use of Parseval's identity. This identity asserts equality between the integral of the norm of a periodic function f and the sum of the norm of the function's Fourier coefficients $\mathcal{F}(f)$

$$\frac{1}{2T} \int_{-T}^{T} dt \, |f(t)|^2 = \sum_{n=-\infty}^{\infty} |\mathcal{F}(f)|^2. \tag{55}$$

The effect of the third derivative is to multiply the power spectrum by $(n\Omega)^6$ while at the same time replacing ${}^{(3)}\mathcal{G}_{a_1 a_2}$ by $\mathcal{G}_{a_1 a_2}$. Hence we can write for the radiated power in the n-th harmonic of the orbital angular frequency

$$P_n = 2 \times \frac{8\pi}{75} (n\Omega)^6 \sum_{m=-2}^{2} \left| \mathcal{F} \left(\mathcal{G}_{a_1 a_2} \left(\mathcal{Y}_{a_1 a_2}^{2m} \right)^* \right) \right|^2 \tag{56}$$

$$= \frac{1}{15} (n\Omega)^6 \, \mu^2 \, \Psi, \tag{57}$$

where

$$\Psi = \left| 2a^2 e \, \mathcal{F}(\cos(u)) - \frac{1}{2}\mathcal{F}(\cos(2u)) \left(a^2 - b^2\right) \right|^2$$

$$+ 3 \left| -2a^2 e \, \mathcal{F}(\cos(u)) + \frac{1}{2}\mathcal{F}(\cos(2u)) \left(a^2 + b^2\right) \right|^2 \tag{58}$$

$$+ 12 \left| -abe \, \mathcal{F}(\sin(u)) + \frac{ab}{2}\mathcal{F}(\sin(2u)) \right|^2 .$$

The factor 2 appearing in equation (56) accounts for the counting of the negative terms in the sum (55). We now proceed with the calculation of the Fourier coefficients of $\sin(mu)$

$$\mathcal{F}(\sin(mu)) = \frac{1}{2\pi} \int_{-\pi}^{\pi} d\beta \, \sin(mu) \, e^{-in\beta}$$

$$= -\frac{1}{2in\pi} \int_{-\pi}^{\pi} du \, \frac{d}{du}\left(e^{-in\beta}\right) \sin(mu)$$

$$= \frac{m}{2in\pi} \int_{-\pi}^{\pi} du \, e^{-in\beta} \, \cos(mu)$$

$$= \frac{m}{2in\pi} \int_{-\pi}^{\pi} du \, \cos(n\beta) \, \cos(mu)$$

$$= \frac{m}{in\pi} \int_{0}^{\pi} du \, \cos(mu) \, \cos(nu - ne\sin u)$$

$$= \frac{m}{2in} \int_{0}^{\pi} \frac{du}{\pi} \left[\cos(u(n+m) - ne\sin u) + \cos(u(n-m) - ne\sin u)\right] .$$

By using the following integral representation of the Bessel functions of the first kind

$$J_n(z) = \int_{0}^{\pi} \frac{du}{\pi} \cos(nu - z\sin u), \tag{59}$$

we arrive at

$$\mathcal{F}(\sin(mu)) = \frac{m}{2in} \left[J_{n+m}(ne) + J_{n-m}(ne)\right]. \tag{60}$$

A similar calculation gives

$$\mathcal{F}(\cos(mu)) = \frac{m}{2n} \left[-J_{n+m}(ne) + J_{n-m}(ne)\right]. \tag{61}$$

By the use of the recurrence relations

$$J_{n-1}(z) + J_{n+1}(z) = \frac{2n}{z} J_n(z), \tag{62}$$

$$J_{n-1}(z) - J_{n+1}(z) = 2J_n'(z), \tag{63}$$

we can express the Fourier coefficients entirely in terms of J_n and its derivative.

We obtain

$$\mathcal{F}(\sin(u)) = \frac{1}{ine} J_n(ne),$$

$$\mathcal{F}(\cos(u)) = \frac{1}{n} J'_n(ne),$$

$$\mathcal{F}(\sin(2u)) = \frac{1}{in} \left[\left(\frac{4}{e^2} - 2 \right) J_n(ne) - \frac{4}{ne} J'_n(ne) \right],$$

$$\mathcal{F}(\cos(2u)) = \frac{1}{n} \left[\frac{4}{e} J'_n(ne) - \frac{4}{ne^2} J_n(ne) \right].$$

(64)

We can insert the above Fourier coefficients into expression (58) and we obtain after rearranging

$$
\begin{aligned}
P_n = {} & \frac{16}{15} \frac{n^2 \Omega^6}{e^4} \mu^2 \\
& \times \Big\{ J_n^2(ne) \left[a^4 + b^4 + a^2 b^2 \left(1 + 3n^2 - 6n^2 e^2 + 3n^2 e^4 \right) \right] + \\
& \quad J'^2_n(ne) \left[a^4 \left(e^6 n^2 + n^2 e^2 - 2e^4 n^2 \right) + b^4 n^2 e^2 + a^2 b^2 \left(n^2 e^2 + 3e^2 - e^4 n^2 \right) \right] + \\
& \quad J_n(ne) J'_n(ne) \left[2a^4 \left(ne^3 - ne \right) - 2b^4 ne + a^2 b^2 \left(7ne^3 - 8ne \right) \right] \Big\}.
\end{aligned}
$$

(65)

Parseval's identity allowed us at one stroke to implement the orbital averaging and to decompose the emitted radiation into its harmonics. In appendix (5.1) there is a slightly less straightforward derivation of the frequency spectrum P_n that goes around Parseval's identity.

Hyperbolic orbit $e \geq 1$: The calculation of the frequency spectrum of an hyperbolic orbits follows the same lines as the calculation of the elliptic one. In fact, by an analytic continuation argument one can deduce from equation (65) most of the structure of the hyperbolic frequency spectrum. However, we will first close our eyes to this fact and present a detailed outline of the calculation. In the end we argue how the result could have been inferred from the elliptic case.

We parametrize the coordinates on an hyperbolic orbit as

$$x = a(e - \cosh u),$$ (66)

$$y = b \sinh u,$$ (67)

where u satisfies the hyperbolic Kepler equation

$$e \sinh(u) - u = \Omega t \equiv \frac{\omega}{\nu} t.$$ (68)

The second mass moment (23) has thus the form

$$
\mathcal{G} = \mu \begin{bmatrix} a^2 (e - \cosh u)^2 & ab(e - \cosh u) \sinh u & 0 \\ ab(e - \cosh u) \sinh u & b^2 \sinh^2 u & 0 \\ 0 & 0 & 0 \end{bmatrix}
$$ (69)

$$
= \mu \begin{bmatrix} a^2 (e^2 - 2e \cosh u + \frac{1}{2} \cosh(2u) + \frac{1}{2}) & ab(e \sinh u - \frac{1}{2} \sinh(2u)) & 0 \\ ab(e \sinh u - \frac{1}{2} \sinh(2u)) & \frac{b^2}{2} \cosh(2u) - \frac{b^2}{2} & 0 \\ 0 & 0 & 0 \end{bmatrix}.
$$ (70)

We can decompose the total radiated energy in the frequency domain as follows

$$E = \frac{8\pi}{75} \int_{-\infty}^{\infty} dt \sum_{m=-2}^{2} \left| {}^{(3)}\mathcal{G}_{a_1 a_2} \left(\mathcal{Y}_{a_1 a_2}^{2m} \right)^* \right|^2 \tag{71}$$

$$= \frac{1}{2\pi} \frac{8\pi}{75} \int_{-\infty}^{\infty} d\omega \sum_{m=-2}^{2} \left| \left[{}^{(3)}\mathcal{G}_{a_1 a_2} \widehat{\left(\mathcal{Y}_{a_1 a_2}^{2m} \right)^*} \right] \right|^2 \tag{72}$$

$$\equiv \frac{1}{2\pi} \int_{-\infty}^{\infty} d\omega \, P(\omega) = \frac{1}{\pi} \int_{0}^{\infty} d\omega \, P(\omega), \tag{73}$$

where the second equality follows from Plancherel's theorem and the hat represents the Fourier transform. We can take the derivative

$$P(\omega) = \frac{8\pi}{75} \omega^6 \sum_{m=-2}^{2} \left| \left(\mathcal{Y}_{a_1 a_2}^{2m} \right)^* \widehat{\mathcal{G}_{a_1 a_2}} \right|^2, \tag{74}$$

and it remains to calculate the Fourier transform of $\mathcal{G}_{a_1 a_2}$, that is

$$\widehat{\mathcal{G}_{a_1 a_2}} = \int_{-\infty}^{\infty} du \, \frac{dt(u)}{du} \, e^{-i\omega t(u)} \, \mathcal{G}_{a_1 a_2}$$

$$= -\frac{1}{i\omega} \int_{-\infty}^{\infty} du \, \frac{d}{du} \left(e^{-i\omega t(u)} \right) \mathcal{G}_{a_1 a_2}.$$

We will outline the remaining calculation for the $\sinh(nu)$ terms

$$\widehat{\sinh(nu)} = -\frac{1}{i\omega} \int_{-\infty}^{\infty} du \, \frac{d}{du} \left(e^{-i\omega t(u)} \right) \sinh(nu)$$

$$= \frac{n}{i\omega} \int_{-\infty}^{\infty} du \, e^{-i\omega t(u)} \cosh(nu)$$

$$= \frac{n}{2i\omega} \int_{-\infty}^{\infty} du \, e^{-i\nu(e \sinh u - u)} \left(e^{nu} + e^{-nu} \right)$$

$$= \frac{n}{2i\omega} \int_{-\infty}^{\infty} du \left(e^{-i\nu e \sinh u + (i\nu + n)u} + e^{-i\nu e \sinh u + (i\nu - n)u} \right).$$

This result can be expressed in terms of modified Bessel functions of the second kind $K_\alpha(x)$. One possible integral representation of $K_\alpha(x)$ has the form (see e.g. page 182 in the Bessel function treatise [10])

$$K_\alpha(x) = \frac{1}{2} e^{\frac{1}{2}\alpha\pi i} \int_{-\infty}^{\infty} dt \, e^{-ix \sinh t + \alpha t}. \tag{75}$$

With this we can write [1]

$$\widehat{\sinh(nu)} = \frac{n}{i\omega} e^{\frac{1}{2}\nu\pi} e^{-\frac{1}{2}n\pi i} \left[K_{i\nu+n}(\nu e) + e^{i\pi n} K_{i\nu-n}(\nu e) \right]. \tag{76}$$

For the relevant terms for $\widehat{\mathcal{G}_{a_1 a_2}}$ we get

$$\widehat{\sinh(u)} = -\frac{1}{\omega} e^{\frac{1}{2}\nu\pi} \left[K_{i\nu+1}(\nu e) - K_{i\nu-1}(\nu e) \right], \tag{77}$$

$$\widehat{\sinh(2u)} = -\frac{2}{i\omega} e^{\frac{1}{2}\nu\pi} \left[K_{i\nu+2}(\nu e) + K_{i\nu-2}(\nu e) \right]. \tag{78}$$

[1] Strictly speaking, when $\text{Re}(\alpha) \in \mathbb{Z}$, the function $K_\alpha(x)$ has to be interpreted as the limiting value $\lim_{\beta \to \alpha} K_\beta(x)$ for $\text{Re}(\beta) \in \mathbb{R} \setminus \mathbb{Z}$.

The calculation of $\widehat{\cosh(nu)}$ proceeds the same way and one finds

$$\widehat{\cosh(nu)} = \frac{n}{i\omega} e^{\frac{1}{2}\nu\pi} e^{-\frac{1}{2}n\pi i} \left[K_{i\nu+n}\left(\nu e\right) - e^{i\pi n} K_{i\nu-n}\left(\nu e\right) \right], \tag{79}$$

so that we have

$$\widehat{\cosh(u)} = -\frac{1}{\omega} e^{\frac{1}{2}\nu\pi} \left[K_{i\nu+1}\left(\nu e\right) + K_{i\nu-1}\left(\nu e\right) \right], \tag{80}$$

$$\widehat{\cosh(2u)} = -\frac{2}{i\omega} e^{\frac{1}{2}\nu\pi} \left[K_{i\nu+2}\left(\nu e\right) - K_{i\nu-2}\left(\nu e\right) \right]. \tag{81}$$

We can now use the recurrence relations

$$K_\alpha(x) = -\frac{x}{2\alpha}[K_{\alpha-1}(x) - K_{\alpha+1}(x)], \tag{82}$$

$$K'_\alpha(x) = -\frac{1}{2}[K_{\alpha-1}(x) + K_{\alpha+1}(x)], \tag{83}$$

to derive the following identities

$$K_{\alpha+2}(x) + K_{\alpha-2}(x) = \left(\frac{4\alpha^2}{x^2} + 2 \right) K_\alpha(x) - \frac{4}{x} K'_\alpha(x), \tag{84}$$

$$K_{\alpha+2}(x) - K_{\alpha-2}(x) = -\frac{4\alpha}{x} K'_\alpha(x) + \frac{4\alpha}{x^2} K_\alpha(x). \tag{85}$$

Combining the above we arrive at

$$
\begin{aligned}
\widehat{\sinh(u)} &= -\frac{2i}{\omega e} e^{\frac{1}{2}\nu\pi} K_{i\nu}\left(\nu e\right), \\
\widehat{\sinh(2u)} &= -\frac{2}{i\omega} e^{\frac{1}{2}\nu\pi} \left[\left(\frac{-4}{e^2} + 2 \right) K_{i\nu}\left(\nu e\right) - \frac{4}{\nu e} K'_{i\nu}\left(\nu e\right) \right], \\
\widehat{\cosh(u)} &= \frac{2}{\omega} e^{\frac{1}{2}\nu\pi} K'_{i\nu}\left(\nu e\right), \\
\widehat{\cosh(2u)} &= \frac{8}{e\omega} e^{\frac{1}{2}\nu\pi} \left[K'_{i\nu}\left(\nu e\right) - \frac{1}{\nu e} K_{i\nu}\left(\nu e\right) \right].
\end{aligned}
\tag{86}
$$

From equation (74) for the radiated power in the frequency domain we find

$$P(\omega) = \frac{1}{30} \omega^6 \mu^2 \Pi, \tag{87}$$

where

$$
\begin{aligned}
\Pi = & \left| 2a^2 e\, \widehat{\cosh(u)} - \frac{1}{2} \widehat{\cosh(2u)} \left(a^2 + b^2\right) \right|^2 \\
& + 3 \left| -2a^2 e\, \widehat{\cosh(u)} + \frac{1}{2} \widehat{\cosh(2u)} \left(a^2 - b^2\right) \right|^2 \\
& + 12 \left| abe\, \widehat{\sinh(u)} - \frac{ab}{2} \widehat{\sinh(2u)} \right|^2.
\end{aligned}
\tag{88}
$$

By plugging in the explicit expressions of the Fourier transforms (86), we can bring $P(\omega)$ into a similar form as (65). We obtain after factoring out terms

$$
\begin{aligned}
P(\omega) = {} & \frac{64}{30} \frac{\omega^2}{e^4} \mu^2 \exp(\nu\pi) \\
& \times \Big\{ K_{i\nu}^2 \left(\nu e\right) \left[(a^4 + b^4)\Omega^2 + a^2 b^2 \left(3\omega^2 - 6\omega^2 e^2 + 3\omega^2 e^4 - \Omega^2\right)\right] + \\
& \quad K_{i\nu}'^2 \left(\nu e\right) \left[a^4 \left(e^2\omega^2 + \omega^2 e^6 - 2\omega^2 e^4\right) + b^4 \omega^2 e^2 + a^2 b^2 \left(-\omega^2 e^2 + \omega^2 e^4 + 3\Omega^2 e^2\right)\right] + \\
& \quad K_{i\nu}\left(\nu e\right) K_{i\nu}'\left(\nu e\right) \left[2a^4 \left(e^3 - e\right)\omega\Omega - 2b^4 \omega\Omega e + a^2 b^2 \left(-7e^3 + 8e\right)\omega\Omega\right] \Big\}.
\end{aligned}
\tag{89}
$$

The similarity of the calculation and final expressions of the elliptic and hyperbolic case should not be regarded as a surprise. In fact, for a deduction of the hyperbolic frequency spectrum from the elliptic one, it suffices to modify the calculation of the elliptic case as follows:

1. The hyperbolic Kepler equation (68) is obtained from the elliptic one (equation (50)) by setting $u \mapsto iu$ and $\Omega \mapsto -i\Omega$. Hence $\sin(nu) \mapsto i\sinh(nu)$ and $\cos(nu) \mapsto i\cosh(nu)$.

2. The Fourier coefficients become Fourier transforms and $n\Omega \mapsto \omega$.

3. The energy radiated per orbit into the n-th harmonic, i.e. $E(n) = \frac{2\pi}{\Omega}P(n)$, becomes the total energy radiated into the n-th harmonic.

The power emitted at zero frequency is non-zero for $e > 1$. To see this, we expand $K_0\left(\nu e\right)$ and $K_0'\left(\nu e\right)$ to first order in ν around $\nu = 0$. Mathematica gives

$$
K_0\left(\nu e\right) = -\gamma - \log\left(\frac{e}{2}\right) - \log(\nu) + \mathcal{O}(\nu^2),
\tag{90}
$$

$$
K_0'\left(\nu e\right) = -\frac{1}{e\nu} + \frac{e\nu}{4}\left(1 - 2\gamma - 2\log\left(\frac{e}{2}\right) - 2\log(\nu)\right) + \mathcal{O}(\nu^2),
\tag{91}
$$

where γ denotes Euler's constant. Inserting the above expressions into equation (88) and then taking the limit of equation (87) towards $\omega = 0$ gives

$$
\lim_{\omega \to 0} P(\omega) = \frac{32}{5} \frac{\mu^2 M^2 (e^2 - 1)}{a^2 e^4}.
\tag{92}
$$

In figure (1) we plot the frequency spectrum (89) for eccentricities ranging from $e = 1$ to $e = 2$. Both the value of the frequency $\bar{\omega}$, where $P(\bar{\omega})$ is maximal, and the value $P(\bar{\omega})$ decrease with increasing hyperbolicity. Although it is not clearly visible in the figure, the power emitted at zero frequency is zero for $e = 1$ and is non-zero for $e > 1$.

19

2.3 Formation of binaries through gravitational wave capture

When two black holes on an hyperbolic trajectory have a near encounter, they may release sufficiently energy through gravitational waves to form a bound binary system.

In the center of mass system, the initial energy of two non-interacting masses is $E_{\mathrm{ini}} = \frac{\mu v^2}{2} = \frac{\mu M (e^2-1)^{1/2}}{2b}$, while the angular momentum of the system is $\mu v b$. Conservation of energy and angular momentum of the system before and after the transition from an hyperbolic to an elliptic orbit gives the equations

$$E_{\mathrm{fin}} = E_{\mathrm{ini}} - E_{\mathrm{GW}}, \tag{93}$$

$$L_{\mathrm{fin}} = \mu v b - L_{\mathrm{GW}}, \tag{94}$$

where the rightmost terms are the released energy through gravitational waves during an hyperbolic encounter (equation (36)) and the amount of angular momentum lost during an hyperbolic encounter (equation (44)) respectively. For there to form a bound binary system, the energy after the encounter E_{fin} must be negative. By the use of the hyperbolic orbit parameters, we can write E_{GW} in terms of μ, M, e and b. Then we can obtain from the condition $E_{\mathrm{ini}} = E_{\mathrm{GW}}$ the maximal impact parameter for capture b_{max} as a function of μ, M and e. It is

$$b_{\mathrm{max}} = \left(\frac{4\mu^2 \varrho(e)^2}{M} \right)^{1/5} \frac{(e-1)^{1/2}}{(e+1)^{9/10} \, |1-e|^{7/5}}. \tag{95}$$

In figure (2) we plot the maximal impact parameter for capture as a function of the eccentricity for binary systems with different mass ratios. We see that the disk of capture decreases as the eccentricity increases and increases as the mass ratio increases. When captured, the orbital semi-major axis after the encounter is

$$a_0 = \frac{\mu M}{2|E_{\mathrm{fin}}|}, \tag{96}$$

while the orbital eccentricity after the encounter reads

$$e_0^2 - 1 = \frac{2E_{\mathrm{fin}} L_{\mathrm{fin}}^2}{M^2 \mu^3}. \tag{97}$$

2.4 Orbital evolution equations for binaries on elliptic orbits

The orbital parameters of a binary system are affected due to the release of gravitational waves. We derive the evolution equations of the semi-major axis and the eccentricity for binaries on an elliptic Keplerian orbit.

Substituting the energy loss equation (38) into the evolution equation (13) one finds the gravitational wave driven evolution of the semi-major axis

$$\frac{da}{dt} = -\frac{64}{5} \frac{\mu M_{\mathrm{tot}}^2}{a^3} \frac{1}{(1-e^2)^{7/2}} \left(1 + \frac{73}{24}e^2 + \frac{37}{96}e^4 \right). \tag{98}$$

Substituting both (38) and (47) into the evolution equation (15) one finds the gravitational wave driven evolution of the orbital eccentricity

$$\frac{de}{dt} = -\frac{304}{15}\frac{\mu M_{\rm tot}^2}{a^4}\frac{e}{(1-e^2)^{5/2}}\left(1+\frac{121}{304}e^2\right). \tag{99}$$

Combining equations (98) and (99) gives

$$\frac{da}{de} = \frac{12}{19}\frac{a}{e}\frac{1+(73/24)e^2+(37/96)e^4}{(1-e^2)\left(1+\frac{121}{304}e^2\right)}. \tag{100}$$

The solution of the differential equation (100) is

$$a(e) = c_0\frac{e^{12/19}}{1-e^2}\left(1+\frac{121}{304}e^2\right)^{870/2299}, \tag{101}$$

where c_0 depends on the initial semi-major axis a_0 and the initial orbital eccentricity e_0. By requiring $a(e_0) = a_0$, we can set

$$c_0 = a_0\left(1-e_0^2\right)e_0^{-12/19}\left(1+\frac{121}{304}e_0^2\right)^{-\frac{870}{2299}}.$$

From the orbit equation (1) we can determine the orbital frequency as a function of the eccentricity

$$\frac{\omega}{\omega_0} = \left[\left(\frac{e}{e_0}\right)^{\frac{12}{19}}\frac{1-e_0^2}{1-e^2}\left(\frac{1+\frac{121}{304}e^2}{1+\frac{121}{304}e_0^2}\right)^{\frac{870}{2299}}\right]^{-3/2}, \tag{102}$$

with the initial orbital frequency $\omega_0 = \sqrt{\frac{M}{a_0^3}}$.

To find the time to coalescence τ we can integrate the inverse to equation (99) by requiring that $e(\tau) = 0$, for at coalescence the eccentricity goes to zero. The time to merger is thus given by the integral

$$\tau = \frac{15}{304}\frac{1}{\mu M_{\rm tot}^2}\int_0^{e_0}de\, a(e)^4\frac{(1-e^2)^{5/2}}{e}\left(1+\frac{121}{304}e^2\right)^{-1} \tag{103}$$

$$= \frac{15}{304}\frac{1}{\mu M_{\rm tot}^2}c_0^4\int_0^{e_0}de\,\frac{e^{29/19}}{(1-e^2)^{3/2}}\left(1+\frac{121}{304}e^2\right)^{1181/2299}. \tag{104}$$
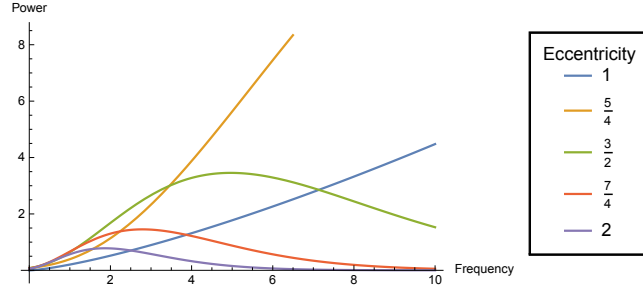
Figure 1: The frequency spectrum of the power emitted by gravitational waves from two masses ($q = 0.5$) during an hyperbolic encounter with eccentricities ranging from $e = 1$ to $e = 2$. A unit system is used where $G = c = M = 1$.
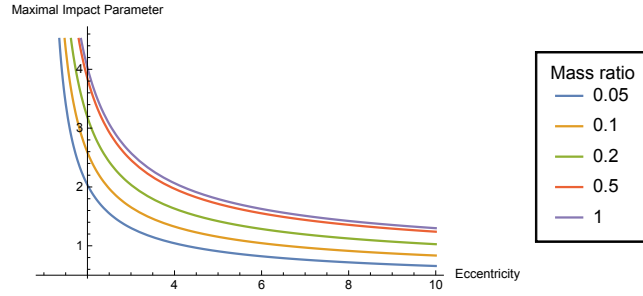

Figure 2: Maximal impact parameter for gravitational wave capture as a function of the eccentricity of the initially hyperbolic orbit. A unit system is used where $G = c = M = 1$.

3 Binary Black Holes in gaseous environments

3.1 Disk - BBH dynamics

We assume the binary to be embedded in a gaseous disk. The interaction between the binary system and the gaseous disk in which it is embedded is complicated and several mechanisms are at play. Examining the dynamics without resorting to hydrodynamical simulations seems unfruitful.

At some point, the tidal torques exerted by the binary onto the disc are sufficiently high to repel gas away from the binary, thus clearing a cavity around the binary. Furthermore, the binary may then be surrounded by a circumbinary disc which affects the orbital evolution of the central binary. The disc-binary interaction drives the binary ultimately into the phase of GWs-driven inspiral, where loss of orbital energy and angular momentum is due to the emission of gravitational waves.

3.1.1 Simplified model of AGN

In the setup of the disk we make many simplifying assumptions. We assume that the disk is axial-symmetric, is geometrically thin and that it is not self-gravitating. The last assumptions means that the motion of the gas may be approximated as being Keplerian, that is, $\Omega = \left(\frac{M_*}{r^3}\right)^{1/2}$, where M_* is the mass of the central object.

The equation for hydrostatic equilibrium in the vertical direction for a geometrically thin disk in a central gravitational potential is

$$\frac{dp}{dz} = -\rho \frac{M_* z}{r^3},\tag{105}$$

where $p(r, z)$ and $\rho(r, z)$ are the pressure and mass density at radius r and height z. We assume the disk to be isothermal in the vertical direction; this amounts to setting $c_s^2 = \frac{p}{\rho}$, where c_s is the sound speed (independent of z). Hence we obtain for the mass density

$$\rho = \rho_0 e^{-\frac{z^2}{2h^2}},\tag{106}$$

with the density at the equatorial plane ρ_0 and with the disk scale height

$$h = \frac{c_s r^{3/2}}{M_*^{1/2}} = \frac{c_s}{\Omega}.\tag{107}$$

The total mass enclosed within a radius r is denoted by $M(r)$ and is related to the surface density $\Sigma(r)$ through $\frac{dM(r)}{dr} = 2\pi r \Sigma(r)$. In the AGN model outlined in Thompson _et al._ [11], the disk mass $M(r)$ is set to $2\sigma^2 r$, where σ stands for the velocity dispersion of the gas. The associated surface density is then

$$\Sigma(r) = \frac{\sigma^2}{\pi r}.\tag{108}$$

Furthermore, the following relations are imposed to the disk data

$$\frac{f_g}{2^{3/2}} = \frac{h}{r} = \frac{1}{\sqrt{2}}\frac{c_s}{\sigma},\tag{109}$$

where $f_g = \frac{\Sigma}{\Sigma_g}$ is the total surface density Σ divided by the gas surface density Σ_g. The last relation is a stability criterion.

3.1.2 A little on accretion disks

Viscous Torque in the Disc   Because the angular velocity of the accretion disk varies with radius, a viscous torque is acting on the gas. This torque represents the amount of angular momentum crossing the disk circumference at radius r per unit time due to the action of viscosity. The shear stress is $\tau = \rho(r)\nu r \frac{d\Omega}{dr}$, where ν is the dynamical viscosity and $\rho(r)$ the mass density. This leads to a viscous torque between two neighbouring disk annuli at radius r

$$T_{\mathrm{visc}} = 2\pi r \int dz\, r\tau = 2\pi \nu \Sigma(r) r^3 \frac{d\Omega}{dr}, \tag{110}$$

where $\Sigma(r) = \int dz\, \rho(r)$ is the surface density of the disk. By employing the Keplerian orbital frequency it follows that the torque is

$$T_{\mathrm{visc}} = -3\pi \nu \Sigma(r) r^2 \Omega(r). \tag{111}$$

One may employ the $\alpha-$disk prescription to parametrize the dynamical viscosity in the case for a thin accretion disk as $\nu = \alpha c_s^2(r)\Omega(r)^{-1}$, where $c_s(r)$ is the local gas sound speed and $0 \leq \alpha \leq 1$ is a dimensionless constant ($\alpha = 0$ corresponds to no accretion). Substituting this expression for ν into the formula for T_{visc} gives

$$T_{\mathrm{visc}} = -3\pi \alpha c_s^2(r)\Sigma(r) r^2. \tag{112}$$

This torque results in an outward transfer of angular momentum.

Continuity equation for accretion disks   Suppose that a gaseous disk has surface density $\Sigma(r)$. The structure and the evolution of gaseous disks can be deduced from the continuity equation

$$2\pi r \frac{\partial \Sigma}{\partial t} = \frac{\partial \dot{M}}{\partial r}, \tag{113}$$

and from angular momentum conservation

$$\frac{\partial(\Omega r^2)}{\partial r}\dot{M} = \frac{\partial}{\partial r}(T_{\mathrm{visc}}). \tag{114}$$

The quantity $\dot{M}(r)$ is the mass flux through the disk at a radius r. Combining equations (113) and (114) gives an evolution equation for the surface density Σ

$$\frac{\partial \Sigma}{\partial t} = \frac{1}{2\pi r}\frac{\partial}{\partial r}\left[\left(\frac{\partial(\Omega r^2)}{\partial r}\right)^{-1}\frac{\partial(T_{\mathrm{visc}})}{\partial r}\right]. \tag{115}$$

We can incorporate external effects acting onto the disk by modifying the viscous evolution equation of the disk: If the disk experiences an external torque per unit mass $\tilde{T}_{\mathrm{ext}}$, the surface density evolution is modified according to

$$\begin{aligned}
\frac{\partial \Sigma}{\partial t} &= \frac{1}{2\pi r}\frac{\partial}{\partial r}\left[\left(\frac{\partial(\Omega r^2)}{\partial r}\right)^{-1}\frac{\partial(T_{\mathrm{visc}})}{\partial r} + \frac{4\pi \Sigma \tilde{T}_{\mathrm{ext}}}{\Omega}\right] \\
&= \frac{1}{2\pi r}\frac{\partial}{\partial r}\left[\left(\frac{\partial(\Omega r^2)}{\partial r}\right)^{-1}\frac{\partial(T_{\mathrm{visc}} + T_{\mathrm{ext}})}{\partial r}\right],
\end{aligned} \tag{116}$$

defining $\frac{\partial T_{\text{ext}}}{\partial r} = 8\pi\Sigma\tilde{T}_{\text{ext}}r$.

3.1.3 A simple model for the disk-binary interaction

Numerical simulations suggest the presence of a depleted cavity inside of which the binary resides. The gas orbiting around this cavity is referred to as the circumbinary disk (CBD). The evolution of the semi-major axis and of the orbital eccentricity are driven by tidal and viscous interactions between the binary and the CBD. We will set up a simplified and idealized model of this picture and see that the phenomena may result in a loss of the binary's orbital angular momentum, a increase in its eccentricity and its faster inspiral.

We thus now assume that a central cavity is surrounded by a CBD. Simulations (references) suggest that in an initially ungapped system the cavity is established after ... binary periods. For simplicity we assume that neither the primary nor the secondary have their own disks. This is also in accordance with Reference, where no inner disks are observed. We aim to relate the viscous angular momentum flux in the inner region of the disk to the orbital evolution of the binary.

The aforementioned numerical simulations (see *e.g.* [12]) suggest that the size of the central cavity extends to about twice the semi-major axis of the binary orbit (as seen from the center of mass frame). This holds for binaries on circular orbits. Artymowicz & Lubow [13] showed through simulations that the location of the inner edge progresses outwards with increasing eccentricity, in their simulations from $r_{\text{in}} \approx 1.9a$ for $e \approx 0.02$ to $r_{\text{in}} \approx 3a$ for $e \approx 0.6$. These findings are also in accordance with simulations performed by Hayasaki *et al.* [14] where for $e = 0.5$ the inner edge was located at $r_{\text{in}} \approx 2.8a$. Also, the above simulations suggest that the gap size seems to be approximately the same for different binary mass ratios q. Inspired by their findings, we thus estimate the inner edge of the circumbinary disk to be set by the twice the distance of the binary at apocenter, *i.e.* $r_{\text{in}} = 2a(1 + e)$, and extrapolate this estimate also to eccentricities up to unity. This is not justified and it is likely that modifications occur for higher eccentricities. Towards more definite answers, one has to admit, there is no way around of performing hydrodynamical simulations. The simulations also show that the cavity is circular shaped, independent of the eccentricity of the binary orbit.

Tidal torques from the binary are expected to act significantly only on a narrow annulus at the inner edge of the CBD and are thus assumed to be zero outside of some cutoff radius r_Λ, which is very similar to r_{in}. Thus the effect of the binary torque on the disk evolution can be accounted for via equation (116) by imposing suitable boundary conditions at the inner edge of the disk. From the previous subsection we deduce

$$\left(\frac{\partial(\Omega r^2)}{\partial r}\right)\dot{M} = \frac{\partial(T_{\text{visc}})}{\partial r} + \left(\frac{\partial(\Omega r^2)}{\partial r}\right)\frac{4\pi\Sigma\tilde{T}_{\text{ext}}}{\Omega}. \tag{117}$$

Integrating from r_b to r_Λ we obtain

$$T_{\text{visc}}(r_\Lambda) = -8\pi\int_{r_b}^{r_\Lambda} dr\, r\Sigma\tilde{T}_{\text{ext}} + 2\int_{r_b}^{r_\Lambda} dr\, r\Omega\dot{M}; \tag{118}$$

we have set $T_{\text{visc}}(r_b) = 0$ because of the clean gap assumption.

The first integral on the right hand side is the total torque the binary exerts on the disk, that is to say, the rate of the angular momentum injection into the disk by the binary. As long as the evolution of the binary is driven predominantly by the tidal coupling to the disk (and not due to the gravitational wave emission) conservation of angular momentum guarantees that this term equals the change of angular momentum of the binary. In the right integral on the right side we can write

$$\dot{M} = 2\pi\Sigma r v_r = 3\pi\Sigma\nu = 3\pi\Sigma\alpha c_s^2/\Omega. \tag{119}$$

Because of the clean gap assumption, the disk surface density Σ is zero for $r < r_{in}$. Thus we approximate the integral by

$$\begin{aligned}
\Delta &\equiv 6\pi\alpha c_s^2 \Sigma(r_{in}) \int_{r_{in}}^{r_\Lambda} dr\, r \\
&= 3\pi\alpha c_s^2 \Sigma(r_{in}) \left[r_\Lambda^2 - r_{in}^2 \right] \\
&\approx 3\pi\alpha c_s^2 \Sigma(r_{in}) \delta r_{in},
\end{aligned}$$

where we set the disk density in the small radial annulus $[r_{\text{in}}, r_\Lambda]$ around the cavity edge to $\Sigma(r_{in})$ since $r_\Lambda - r_{\text{in}} = \delta/2 \ll r_{\text{in}}$ and since we have no model to resolve the surface density of the CBD down to this scale.

From here forward, we will work in the reference frame of the binary system. The binary injects angular momentum into the disk, so we require $\dot{L}_b < 0$. According to this convention, the sign of the viscous torque must be opposite to that of equation (112). In the binary frame, equation (118) therefore translates into

$$T_{\text{visc}}(r_{\text{in}}) = -\dot{L}_b - \Delta, \tag{120}$$

where the viscous torque reads $T_{\text{visc}}(2a(1+e)) = 12\pi\alpha c_s^2 \Sigma a^2 (1+e)^2$. As this term is a few order of magnitudes higher than Δ, we neglect Δ henceforth.

We impose a further assumption to the particular evolution model, that the binary-disk interaction may well be approximated as an adiabatic process (as opposed to an evolution that is driven by sudden perturbations, like the gravitational wave capture scenario of section 2.3). That is to say, we assume that the timescale of the disk-binary interaction is much larger than some characteristic timescale of the binary, like its orbital period. It has to emphasized that this is an idealized assumption; it is somewhat supported by the simulations because they show the maintenance of the circular shape of the cavity across a large spectrum of eccentricities. Under the adiabatic assumption, the change in the binary energy can be related to its change in angular momentum through the orbital frequency,

$$\dot{E}_b = \Omega_b \dot{L}_b. \tag{121}$$

Note that $\dot{L}_b < 0$, so $\dot{E}_b < 0$ and therefore the binary system always evolves toward lower energy. In particular an initially bound orbit always stays on an elliptic orbit. Energy conservation implies that energy is deposited in the circumbinary disk and this dissipated energy may *e.g.* heat up the disk material.

From the evolution equation (13) for the semi-major axis of the binary orbit and the binary energy $E_b = -\frac{\Omega_b L_b}{2\sqrt{1-e^2}}$ it follows

$$\frac{\dot{a}}{a} = -\frac{\dot{E}_b}{E_b} = -\frac{T_{\text{visc}}(r_{\text{in}})}{L_b} 2\sqrt{1-e^2} \tag{122}$$

$$= -2\frac{T_{\text{visc}}(r_{\text{in}})}{\mu \Omega_b a^2}, \tag{123}$$

where the last equation follows by substituting the orbital angular momentum (11). Substituting the explicit formula for the viscous torque results in

$$\dot{a} = -\frac{24\pi a \alpha c_s^2 \Sigma (1+e)^2}{\mu \Omega_b}. \tag{124}$$

Starting from the standard evolution equation (14), we similarly get for the evolution of the eccentricity the expression

$$\dot{e} = \frac{1-e^2}{e}\left(\frac{1}{\sqrt{1-e^2}} - 1\right)\frac{T_{\text{visc}}(r_{\text{in}})}{\mu \Omega_b a^2} \tag{125}$$

$$= \frac{(1+e)^2}{e}(\sqrt{1-e^2} + e^2 - 1)\frac{12\pi \alpha c_s^2 \Sigma}{\mu \Omega_b}. \tag{126}$$

This means that in this model for $a \neq 0$ the semi-major axis decreases in time and the orbital eccentricity doesn't change for $e = 0$ and increases in time for $e \neq 0$. Even though we have $\dot{e} \geq 0$, the orbit cannot become unbound since the orbit's energy is decreasing.

We can divide equation (124) by equation (126) and solve the resulting differential equation. We get

$$a(e) = a_0 \left(\frac{1 - \sqrt{1-e_0^2}}{1 - \sqrt{1-e^2}}\right)^2, \tag{127}$$

with initial semi-major axis a_0 and initial eccentricity e_0.

In chapter (4) we need to insert values for α, Σ and c_s. We set those quantities of the circumbinary disk equal to those of the background disk at the location where the binary resides within the background disk. One may argue that the quantities taken at the inner edge of the CBD should not differ significantly from the quantities taken at the outer edge of the CBD and there those quantities should not differ from their values in the background disk. The inspiration for using this assumption comes from Baruteau *et al.* [15], who use exactly the same assumption for the same problem. We use this same assumption due to the lack of a better alternative.

3.1.4   Shortcomings of the model

The implicit assumption on the disk-binary interaction than goes along by employing equation (121) may be phrased in another way. Namely, that the non-axisymmetric potential perturbations of the binary system are assumed to be

small around the average binary potential. This is certainly fulfilled for circular orbits and also for orbits with low eccentricity. For higher eccentricities there is no good reason why this assumption should hold. But since the hydrodynamical simulations do not show signs of a non-circular cavity shapes even for large eccentricities, we assume the torque to act on average axially-symmetrically onto the disk.

Along the same lines, the use of assumption (121) really reflects our ignorance of the character of the energy flux between the binary and the disk. For a deeper understanding of the energy flux one needs a microscopic understanding of the disk-binary interaction that does not rely on a macroscopic orbital averaging of dynamical parameters. At the level of Hamiltonian dynamics, we assume that the Hamiltonian describing the disk-binary interaction only depends on the angular momentum of the binary. For a more refined and correct treatment of the problem it is necessary to also include the position and momentum coordinates of the binary into the Hamiltonian.

In spite of the above dissatisfaction, similar handling is also found in the literature. Hayasaki [16] uses relation (121) and applies it to eccentric orbits up to eccentricity 1. Goldreich & Sari [17] set up a formalism for planet-disk interaction and while explicitly acknowledging that the results are valid only to lowest order in the eccentricity, they apply it eventually to eccentric orbits up to eccentricity 1.

3.2   Results from the binary evolution channel

From this section onwards, all plots, numerical values and equations are expressed in SI units.

Both gravitational wave emission and the disk interaction affect the evolution of the binary system. To investigate the resulting dynamics, we combine $\dot{a}_{\text{disk-binary}}$ (expression 124)) and $\dot{e}_{\text{disk-binary}}$ (expression 126)) of the disk-driven orbital evolution channel with the corresponding gravitational wave driven evolution equations $\dot{a}_{\text{GW}}$ and $\dot{e}_{\text{GW}}$ of section (2.4). That is, the combined dynamics is described by the evolution equations

$$
\begin{aligned}
\dot{a} &= \dot{a}_{\text{GW}} + \dot{a}_{\text{disk-binary}}, \\
\dot{e} &= \dot{e}_{\text{GW}} + \dot{e}_{\text{disk-binary}}.
\end{aligned}
\tag{128}
$$

We integrate this coupled system of differential equations numerically. Among the various ordinary differential equations solvers in Matlab, the ode23tb function performed best. This solver is designed for solving stiff ordinary differential equations. That the evolution equations exhibit stiffness is not too surprising; during the latest stages of inspiral, the solution does indeed display much variation within a short time interval.

The numerical integration yields the temporal evolution of the semi-major axis and the eccentricity that results from the particular evolution channel (128). Of particular interest is the time to merger of a binary system with initial conditions a_0 and e_0. This time is taken as the abscissa where the numerical solution

$a(t)$ (or $e(t)$) approaches the abscissa axis.

At most values of a the disk-binary interaction dominates the gravitational wave emission. Only at the latest stages of inspiral gravitational emission becomes important. This reduces the purely gravitational wave-driven merger time by several orders of magnitudes. Figure (3) shows, as a function of the initial eccentricity, the purely gravitational wave-driven merger times (blue) and those where in addition disk interactions are taken into account (green). Here we used $M = 50 M_\odot$; $\mu = M/4$; $a_0 = 10$ AU.

The disk-binary dynamics reduces the elliptic binary's semi-major axis while at the same time it increases the elliptic orbit's eccentricity. At a critical semi-major axis, where $\dot{a}_{\mathrm{GW}} = \dot{a}_{\mathrm{disk\text{-}binary}}$, the binary evolution changes from being predominately disk driven to being predominately driven by gravitational wave emission. Figures (4) to (7) display the orbit's semi-major axis as a function of the orbit's eccentricity for different initial data. The disk parameters $\alpha = 0.01$, $\Sigma = 6.2 \times 10^3$ kg/m^3, $c_s = 5 \times 10^3$ m/s remain unchanged and the numerical solution $a(e)$ is plotted

⋄ in Figure (4) for initial eccentricities e_0 ranging from 0.01 to 0.9. The other binary parameters have the values $a_0 = 10$ AU, $M = 50 M_\odot$ and $q = 1$.

⋄ in Figure (5) for initial semi-major axes a_0 ranging from 1 AU to 20 AU. The other binary parameters have the values $e_0 = 0.3$ AU, $M = 50 M_\odot$ and $q = 1$.

⋄ in Figure (6) for binary masses M ranging from $10 M_\odot$ to $50 M_\odot$. The other binary parameters have the values $e_0 = 0.3$, $a_0 = 10$ AU and $q = 1$.

⋄ in Figure (7) for binary masses q ranging from 0.05 to 1. The other binary parameters have the values $e_0 = 0.3$, $a_0 = 10$ AU and $M = 50 M_\odot$.

The eccentricity at the transition semi-major axis (where $\dot{a}_{\mathrm{GW}} = \dot{a}_{\mathrm{disk\text{-}binary}}$) does not necessarily coincide with the maximum eccentricity reached during the orbital evolution. As seen from figure (8), at low initial eccentricities the eccentricity keeps on growing even after gravitational wave emission has taken over. At higher initial eccentricities the eccentricity approaches unity and then rapidly decays due to GW-emission.
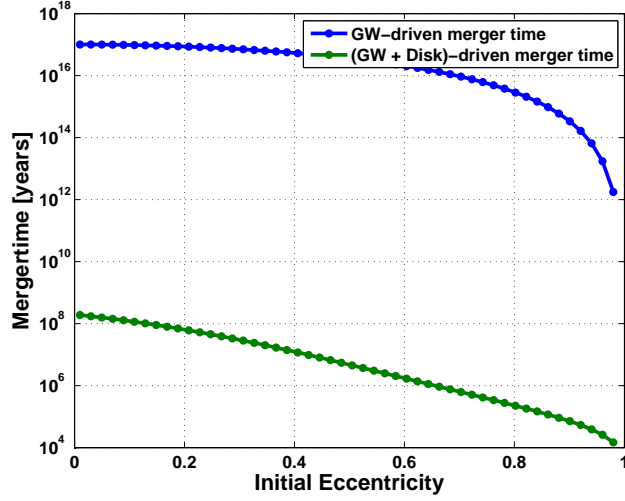
Figure 3: Merger times as a function of the initial binary eccentricity. The blue curve represents the merger times resulting from GW-driven decay, the green one resulting from both GW emission and disk-binary interaction.

Figure 4: Merger times as a function of the initial binary eccentricity. The blue curve represents the merger times resulting from GW-driven decay, the green one resulting from both GW emission and disk-binary interaction.

Figure 5: Merger times as a function of the initial binary eccentricity. The blue curve represents the merger times resulting from GW-driven decay, the green one resulting from both GW emission and disk-binary interaction.
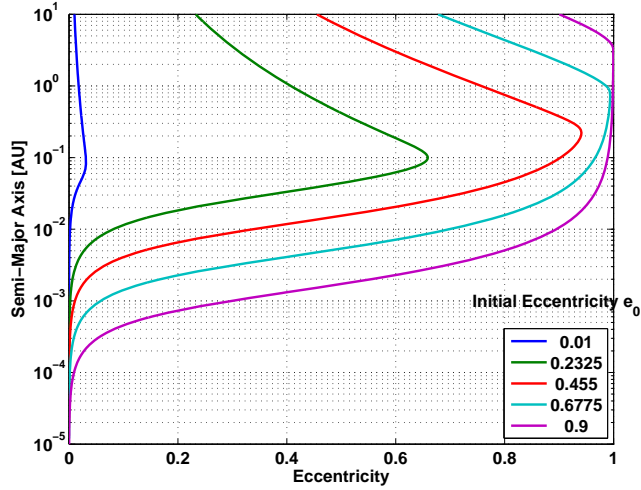

Figure 6: Merger times as a function of the initial binary eccentricity. The blue curve represents the merger times resulting from GW-driven decay, the green one resulting from both GW emission and disk-binary interaction.
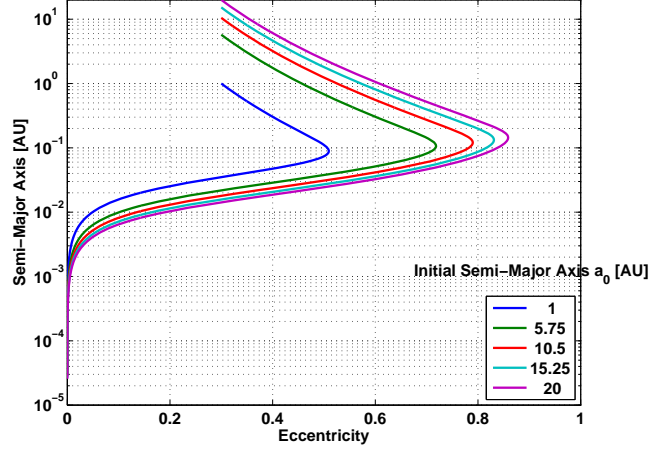
Figure 7: Merger times as a function of the initial binary eccentricity. The blue curve represents the merger times resulting from GW-driven decay, the green one resulting from both GW emission and disk-binary interaction.
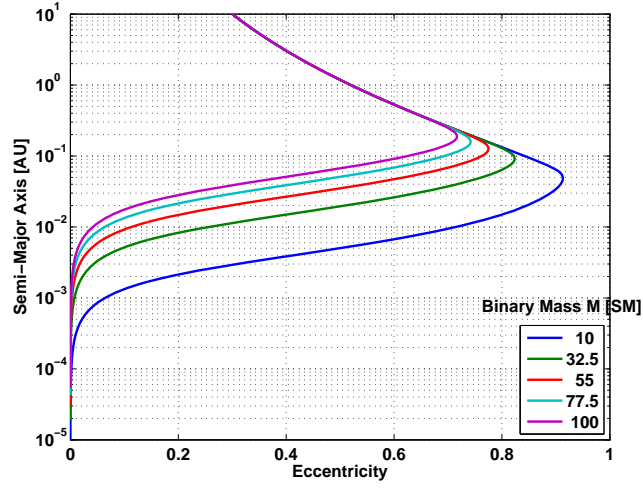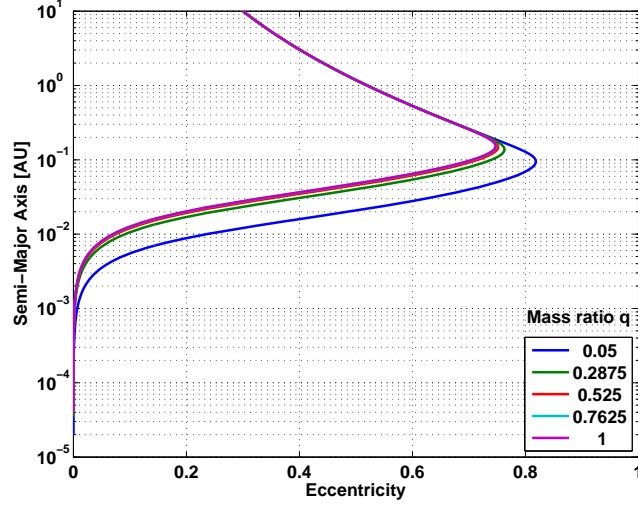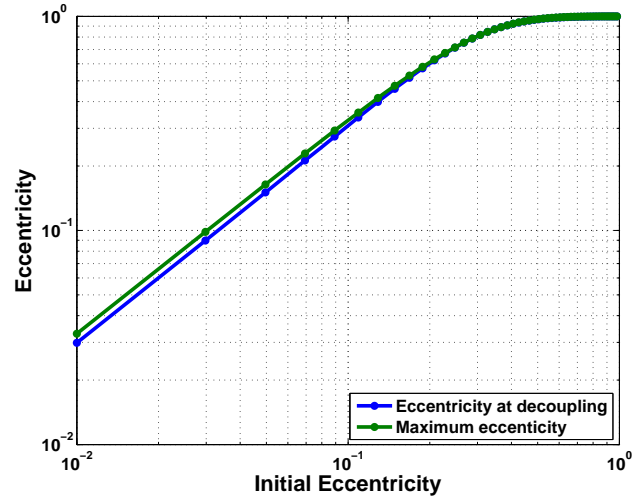

Figure 8: Eccentricity growth.

4 Merger rate density estimation

In this section we want to estimate the binary black hole (BBH) merger rate density that could be expected from the binary evolution channel of the previous chapter. The merger rate density we take as the number of coalescences per unit time per unit volume in the local universe.

We parametrize the rate density of black hole binary mergers in AGN disks in two ways, the second being a refinement of the first. The first parametrization is simply:

$$\mathcal{R}_1 = \frac{N_{\mathrm{BHs}}\, f_b\, f_d\, n_{\mathrm{AGN}}}{\tau_{\mathrm{avg}}}. \tag{129}$$

Here N_{BHs} is the number of stellar mass black holes per nucleus, f_b is the fraction of black holes residing within binaries, f_d is the fraction of black holes embedded in the AGN disk (that is, $N_{\mathrm{BHs}} f_b f_d / 2$ is the number of binary black holes embedded in the disk), n_{AGN} is the number density of active galactic nuclei and τ_{avg} is the average binary merger time. In McKernan *et al.* [18] the prescription (129) is taken as a starting point, however, no attempt is then made to estimate the average merger time of binary systems (it is instead assumed that all binaries merge within the lifetime of the disk).

The second prescription for the rate density is more refined and is determined from a weighted average of several orbital parameters, in the sense described below. The average merger time needed in prescription (129) is obtained from averaging over the data set obtained from the second prescription, so we proceed in setting up the calculation for the latter.

4.1 Mass distributions

We start with an initial stellar distribution. We assume that all stars above a critical mass have evolved into black holes, yielding a BH initial distribution.

Stellar distribution The initial stellar mass distribution seems to follow a multiple power-law function. Here we adopt the initial stellar mass function of Kroupa [19]

$$f_{\mathrm{IMF}}(m) = \begin{cases} k_0 \left(\frac{m}{M_\odot} \right)^{-0.3} & \text{if } m < 0.08 M_\odot \\ k_1 \left(\frac{m}{M_\odot} \right)^{-1.3} & \text{if } 0.08 M_\odot < m < 0.5 M_\odot \, , \\ k_2 \left(\frac{m}{M_\odot} \right)^{-2.3} & \text{if } m > 0.5 M_\odot \end{cases} \tag{130}$$

with normalization parameters $k_0, k_1 = 0.08 k_0$ and $k_2 = 0.04 k_0$. The normalization is taken such that $N_{\mathrm{s,tot}} = \int_{m_{\mathrm{s,min}}}^{m_{\mathrm{s,max}}} dm f_{\mathrm{IMF}}(m)$ and accordingly the parameter k_0 is

$$k_0 = \frac{N_{\mathrm{s,tot}}}{M_\odot} \bigg/ \left[0.56 - \frac{1}{0.7} \left(\frac{m_{\mathrm{s,min}}}{M_\odot} \right)^{0.7} - \frac{0.04}{1.3} \left(\frac{m_{\mathrm{s,max}}}{M_\odot} \right)^{-1.3} \right]. \tag{131}$$

The total stellar mass is

$$M_* = \int_{m_{\mathrm{s,min}}}^{m_{\mathrm{s,max}}} dm\, m f_{\mathrm{IMF}} \tag{132}$$

$$= k_0 M_\odot^2 \left[0.22 - \frac{1}{1.7} \left(\frac{m_{\mathrm{s,min}}}{M_\odot} \right)^{1.7} - \frac{0.04}{0.3} \left(\frac{m_{\mathrm{s,max}}}{M_\odot} \right)^{-0.3} \right]. \tag{133}$$

We adopt the "Nuker law" parametrization ([20]) for the stellar density profile $\rho_*(r)$

$$\rho_*(r) \propto \left(\frac{r_b}{r} \right)^\gamma \left[1 + \left(\frac{r}{r_b} \right)^\alpha \right]^{\frac{\gamma - \beta}{\alpha}}, \tag{134}$$

We simplify this profile by using its asymptomatic slopes,

$$\rho_*(r) = \begin{cases} \rho_0 \left(\frac{r}{r_b} \right)^{-\gamma} & \text{if } r \le r_b; \\ \rho_0 \left(\frac{r}{r_b} \right)^{-\beta} & \text{if } r > r_b \end{cases} ; \tag{135}$$

the parameter α would parameterize the transition between the inner cusp and the outer power law. The break radius r_b is approximately on the order of the radius of influence of the SMBH ([21]), characterized as $r_b = M_{\mathrm{SMBH}}/\sigma^2$ (σ is the stellar dispersion). The normalization parameter ρ_0 can then be expressed as

$$\rho_0 = \frac{M_*}{4\pi r_b^3} \left(\frac{1}{3 - \gamma} - \frac{1}{3 - \beta} \right)^{-1}, \tag{136}$$

where we used the assumption that we only consider models with $\beta > 3$.

BH distribution   If we assume that every star heavier than m_{cr} evolved into a BH, the total initial number of BHs is

$$N = \int_{m_{\mathrm{s,cr}}}^{m_{\mathrm{s,max}}} dm\, f_{\mathrm{IMF}} \tag{137}$$

$$= k_0 M_\odot \left[0.56 - \frac{1}{0.7} \left(\frac{m_{\mathrm{s,cr}}}{M_\odot} \right)^{0.7} - \frac{0.04}{1.3} \left(\frac{m_{\mathrm{s,max}}}{M_\odot} \right)^{-1.3} \right] \tag{138}$$

$$= k M_*, \tag{139}$$

where we defined

$$k = \frac{1}{M_\odot} \frac{\left[0.56 - \frac{1}{0.7} \left(\frac{m_{\mathrm{s,cr}}}{M_\odot} \right)^{0.7} - \frac{0.04}{1.3} \left(\frac{m_{\mathrm{s,max}}}{M_\odot} \right)^{-1.3} \right]}{\left[0.22 - \frac{1}{1.7} \left(\frac{m_{\mathrm{s,min}}}{M_\odot} \right)^{1.7} - \frac{0.04}{0.3} \left(\frac{m_{\mathrm{s,max}}}{M_\odot} \right)^{-0.3} \right]}. \tag{140}$$

The total mass of all BHs is

$$M_{\mathrm{BH}} = \int_{m_{\mathrm{s,cr}}}^{m_{\mathrm{s,max}}} dm\, m\, f_{\mathrm{IMF}}. \tag{141}$$

The BH mass distribution is denoted as $f_{\mathrm{BH}}(m)$ and is normalized such that $\int dm f_{\mathrm{BH}}(m) = 1$. We adopt a Salpeter mass function for the BH distribution

$$f_{\mathrm{BH}}(m) = \xi_0 m^{-2.35}; \tag{142}$$

the normalization parameter ξ_0 is accordingly

$$\xi_0 = -\frac{1.35}{m_{\mathrm{BH,max}}^{-1.35} - m_{\mathrm{BH,min}}^{-1.35}}. \tag{143}$$

If $N(r)$ denotes the total number of BHs inside some radius r, the number dN of BHs lying inside r with masses between m and $m + dm$ is

$$dN = N(r) f_{\mathrm{BH}}(m) dm \tag{144}$$
$$= k M_*(r) f_{\mathrm{BH}}(m) dm, \tag{145}$$

where $M_*(r)$ is the total stellar mass inside radius r $(M_*(\infty) \equiv M_*)$. Note that for the last equality we assumed that the mass distribution of the BHs is independent of the radius at which they reside (an assumption that could be refined, but it is used in the literature, see $e.g$ [22]). We can write dN in the following form

$$dN = dm\, k\, f_{\mathrm{BH}}(m) \int_0^r dr\, \rho_*(r) 4\pi r^2, \tag{146}$$

and this yields finally

$$\frac{dN}{dm} = \begin{cases} k\, f_{\mathrm{BH}}(m)\, \frac{4\pi\rho_0}{3-\gamma} r_b^\gamma r^{3-\gamma} & \text{if } r \leq r_b \\ k\, f_{\mathrm{BH}}(m)\, 4\pi\rho_0 r_b^3 \left[\frac{1}{3-\gamma} + \frac{1}{3-\beta}\left[\left(\frac{r}{r_b}\right)^{3-\beta} - 1 \right] \right] & \text{if } r > r_b \end{cases} . \tag{147}$$

The number of BHs with masses between m and $m + dm$ in a radial shell from radius r to $r + dr$ is accordingly

$$\begin{cases} dm\, k\, f_{\mathrm{BH}}(m)\, \frac{4\pi\rho_0}{3-\gamma} r_b^\gamma \left[(r+dr)^{3-\gamma} - r^{3-\gamma} \right] & \text{if } r \leq r_b \\ dm\, k\, f_{\mathrm{BH}}(m)\, \frac{4\pi\rho_0}{3-\beta} r_b^3 \left[\left(\frac{r+dr}{r_b}\right)^{3-\beta} - \left(\frac{r}{r_b}\right)^{3-\beta} \right] & \text{if } r > r_b \end{cases} . \tag{148}$$

The total number of BHs in a radial shell from radius r to $r + dr$ is

$$\begin{cases} k\, \frac{4\pi\rho_0}{3-\gamma} r_b^\gamma \left[(r+dr)^{3-\gamma} - r^{3-\gamma} \right] & \text{if } r \leq r_b \\ k\, \frac{4\pi\rho_0}{3-\beta} r_b^3 \left[\left(\frac{r+dr}{r_b}\right)^{3-\beta} - \left(\frac{r}{r_b}\right)^{3-\beta} \right] & \text{if } r > r_b \end{cases} . \tag{149}$$

4.2 Rate per galactic nucleus

To estimate the merger rate per galactic nucleus, we add up the rate contributions coming from different radial shells. We partition the disk into $\mathcal{I}_r$ intervals (we assume that the disk around the SMBH is truncated at 1 pc). The number of BHs within each radial shell $[j\Delta r, (j+1)\Delta r]$, where $\Delta r = 1\,\mathrm{pc}/|\mathcal{I}_r|$, is obtained from equation (149)

$$N_j = \begin{cases} k\, \frac{4\pi\rho_0}{3-\gamma} r_b^\gamma \left[((j+1)\Delta r)^{3-\gamma} - (j\Delta r)^{3-\gamma} \right] & \text{if } (j+1)\Delta r \leq r_b \\ k\, \frac{4\pi\rho_0}{3-\beta} r_b^3 \left[\left(\frac{(j+1)\Delta r}{r_b}\right)^{3-\beta} - \left(\frac{j\Delta r}{r_b}\right)^{3-\beta} \right] & \text{if } j\Delta r > r_b \end{cases} . \tag{150}$$

The mean radius of a radial shell is

$$r_j = (j + 0.5)\Delta r. \tag{151}$$

The number of BBHs within each radial shell that are embedded in the disk is given by

$$N_{\mathrm{BBH},j} = \frac{N_j f_b f_d}{2}. \tag{152}$$

4.2.1 BBH distributions in a radial shell

In each radial shell we distribute the number of BBHs within this shell for every binary parameter (m_1, m_2, e_0, a_0) according to some canonical binary parameter distribution functions. We assume for simplicity that the binary parameter distributions are independent from each other. The distributions in this subsection refer to a single radial shell $[j\Delta r, (j+1)\Delta r]$.

Primary mass distribution   We adopt the initial mass function of Salpeter for the primary mass distribution. Thus, in a radial shell $[j\Delta r, (j+1)\Delta r]$, the number of binaries with primary mass between m and $m + dm$ is given by

$$\frac{f_b f_d}{2} dm\, k\, f_{\mathrm{BH}}(m) \begin{cases} \frac{4\pi\rho_0}{3-\gamma} r_b^\gamma \left[((j+1)\Delta r)^{3-\gamma} - (j\Delta r)^{3-\gamma} \right] & \text{if } (j+1)\Delta r \le r_b \\ \frac{4\pi\rho_0}{3-\beta} r_b^3 \left[\left(\frac{(j+1)\Delta r}{r_b} \right)^{3-\beta} - \left(\frac{j\Delta r}{r_b} \right)^{3-\beta} \right] & \text{if } j\Delta r > r_b \end{cases}. \tag{153}$$

Secondary mass distribution   The secondary mass distribution is determined by the distribution of the mass ratio q, assumed to follow a uniform distribution (see Tout *et al.* [23] or Ablimit & Maeda [24])

$$f(q) = \mu_0, \tag{154}$$

where μ_0 is a constant and $0.1 \le q \le 1$. From the normalization condition $\mu_0 \int_{0.1}^1 dq = N_{\mathrm{BBH},j}$ we extract $\mu_0 = \frac{10}{9} N_{\mathrm{BBH},j}$.

Orbital separation distribution   The distribution of the initial orbital separation a_0 is assumed to be logarithmically flat (see again [23],[24])

$$f(a_0) = \chi_0/a_0, \tag{155}$$

between the limits 0.1 AU and 500 AU. Normalizations gives $\chi_0 = \frac{N_{\mathrm{BBH},j}}{\log 5000}$.

Orbital eccentricity distribution   We choose the distribution of the initial orbital eccentricity e_0 to follow a thermal distribution (see [23])

$$f(e_0) = \varsigma_0 e_0, \tag{156}$$

between the limits 0 and 1. Normalization gives $\varsigma_0 = 2N_{\mathrm{BBH},j}$.

4.2.2 Calculation of rate within a radial shell

We have set up everything to finally perform the calculation of the rate of coalescences in a radial shell. To this end, we partition each binary parameter into bins and distribute $N_{\mathrm{BBH},j}$, the total number of BBHs within a shell, among the different bins. The merger rate is then ascertained as follows:

The sets $\mathcal{I}_x$ (where x is one of M, q, e_0 or a_0) will denote the number of bins for the corresponding binary distributions x. The numbers $N_{x,i}$ will provide the number of BBHs residing within the bin $i \in \mathcal{I}_x$ of the binary distribution x. We need to take all possible combinations of the bins $\mathcal{I}_M$, $\mathcal{I}_q$, $\mathcal{I}_{a_0}$ and $\mathcal{I}_{e_0}$ and calculate for each such combination the binary's merger time based on the evolution equations (128). We denote such a combination by $\alpha \in \mathcal{I}_M \times \mathcal{I}_q \times \mathcal{I}_{a_0} \times \mathcal{I}_{e_0}$ and the merger time corresponding to this combination by $\tau_{\mathrm{merger},\alpha}$. We take as the input values needed for the numerical calculation of the merger time the average quantities x_i of the orbital parameter x in bin i. The total number of BBHs inhabiting a combination $\alpha = (k, l, u, v)$ is given by $N_{M,k} N_{q,l} N_{a_0,u} N_{e_0,v} / N_{\mathrm{BBH},j}^3 \equiv N_\alpha / N_{\mathrm{BBH},j}^3$. The total merger rate resulting from a radial shell labelled by j is therefore

$$\mathcal{R}_j = \sum_\alpha \frac{N_\alpha}{N_{\mathrm{BBH},j}^3} \frac{1}{\tau_{\mathrm{merger},\alpha}}, \tag{157}$$

where the sum goes over all $\alpha \in \mathcal{I}_M \times \mathcal{I}_q \times \mathcal{I}_{a_0} \times \mathcal{I}_{e_0}$.

It remains to write down the expressions $N_{x,i}$ and x_i for a bin $i \in \mathcal{I}_x$ of the binary parameter x.

Primary mass The number of primary BHs within the mass bin $[m_{\mathrm{BH,min}} + i\Delta M, m_{\mathrm{BH,min}} + (i+1)\Delta M]$, where $\Delta M = (m_{\mathrm{BH,max}} - m_{\mathrm{BH,min}})/|\mathcal{I}_M|$ and $i \in \mathcal{I}_M$, is obtained by integrating equation (153) with respect to m

$$N_{M,i} = \frac{f_b f_d}{2} \frac{4\pi k \rho_0 \xi_0}{1.35} \left[(m_{\mathrm{BH,min}} + i\Delta M)^{-1.35} - (m_{\mathrm{BH,min}} + (i+1)\Delta M)^{-1.35} \right]$$
$$\times \begin{cases} \frac{1}{3-\gamma} r_b^\gamma \left[((j+1)\Delta r)^{3-\gamma} - (j\Delta r)^{3-\gamma} \right] & \text{if } (j+1)\Delta r \le r_b \\ \frac{1}{3-\beta} r_b^3 \left[\left(\frac{(j+1)\Delta r}{r_b} \right)^{3-\beta} - \left(\frac{j\Delta r}{r_b} \right)^{3-\beta} \right] & \text{if } j\Delta r > r_b \end{cases}. \tag{158}$$

The average mass within this mass bin is

$$M_i = \frac{1.35}{0.35} \frac{\left[(m_{\mathrm{BH,min}} + i\Delta M)^{-0.35} - (m_{\mathrm{BH,min}} + (i+1)\Delta M)^{-0.35} \right]}{\left[(m_{\mathrm{BH,min}} + i\Delta M)^{-1.35} - (m_{\mathrm{BH,min}} + (i+1)\Delta M)^{-1.35} \right]}. \tag{159}$$

Mass ratio The number of BBH within the mass ratio bin $[0.1 + i\Delta q, 0.1 + (i+1)\Delta q]$, where $\Delta q = 0.9/|\mathcal{I}_q|$ and $i \in \mathcal{I}_q$, is

$$N_{q,i} = \mu_0 \Delta q. \tag{160}$$

The average mass ratio within this mass ratio bin is

$$q_i = (i + 0.5)\Delta q + 0.1. \tag{161}$$

Orbital separation   The number of BBH within the orbital separation bin $[0.1\text{AU}+i\Delta a, 0.1\text{AU}+(i+1)\Delta a]$, where $\Delta a = 499.9\text{AU}/|\mathcal{I}_{a_0}|$ and $i \in \mathcal{I}_{a_0}$, is

$$N_{a_0,i} = \chi_0 \log\left(\frac{0.1\text{AU} + (i+1)\Delta a}{0.1\text{AU} + i\Delta a}\right). \tag{162}$$

The average a_0 within this bin is

$$a_{0_i} = \frac{\Delta a}{\log\left(\frac{0.01\text{AU}+(i+1)\Delta a}{0.01\text{AU}+i\Delta a}\right)}. \tag{163}$$

Orbital eccentricity   The number of BBH within the eccentricity bin $[i\Delta e_0, (i+1)\Delta e_0]$, where $\Delta e_0 = 1/|\mathcal{I}_{e_0}|$ and $i \in \mathcal{I}_{e_0}$, is

$$N_{e_0,i} = \varsigma_0 \, (i + 0.5) \, (\Delta e_0)^2. \tag{164}$$

The average e_0 within this bin is

$$e_{0_i} = \frac{((i+1)\Delta e_0)^3 - (i\Delta e_0)^3}{3 \, (i+0.5) \, (\Delta e_0)^2}. \tag{165}$$

Parameter dependencies   We resolve for each factor in the radial shell rate (157) the involved parameters:

⋄ τ_{merger} depends on $M_i, q_i, a_{0_i}, e_{0_i}, c_s, \alpha, \Sigma(\sigma, r_j)$.

⋄ $N_{\text{BBH},j}$ and $N_{x,i}$ depend on $f_b, f_d, m_{\text{s,cr}}, m_{\text{BH,min}}, m_{\text{BH,max}}, m_{\text{s,min}}, m_{\text{s,max}}, N_{s,\text{tot}}, M_{\text{SMBH}}, \sigma, \gamma, \beta$.

The explicit expression of a combination $\alpha = (k, l, u, v)$ in the formula (157) has not an illuminating form

$$\frac{N_\alpha}{N_{\text{BBH},j}^3} \frac{1}{\tau_{\text{merger},\alpha}} =$$

$$\times \frac{1}{m_{\text{BH,min}}^{-1.35} - m_{\text{BH,max}}^{-1.35}} \frac{\sigma^6}{M_{\text{SMBH}}^3} \left(\frac{1}{3-\gamma} - \frac{1}{3-\beta}\right)^{-1} \frac{\left[0.56 - \frac{1}{0.7}\left(\frac{m_{\text{s,cr}}}{M_\odot}\right)^{0.7} - \frac{0.04}{1.3}\left(\frac{m_{\text{s,max}}}{M_\odot}\right)^{-1.3}\right]}{\left[0.56 - \frac{1}{0.7}\left(\frac{m_{\text{s,min}}}{M_\odot}\right)^{0.7} - \frac{0.04}{1.3}\left(\frac{m_{\text{s,max}}}{M_\odot}\right)^{-1.3}\right]}$$

$$\times N_{s,\text{tot}} f_b f_d \frac{10}{9} \frac{1}{\log 5000} \Delta q \log\left(\frac{0.1\text{AU} + (u+1)\Delta a}{0.1\text{AU} + u\Delta a}\right) (v+0.5) (\Delta e_0)^2 \frac{1}{\tau_{\text{merger}}(M_k, q_l, a_{0_u}, e_{0_v}, \Sigma(\sigma, r_j))}$$

$$\times \left[(m_{\text{BH,min}} + k\Delta M)^{-1.35} - (m_{\text{BH,min}} + (k+1)\Delta M)^{-1.35}\right]$$

$$\times \begin{cases} \frac{1}{3-\gamma} r_b^\gamma \left[((j+1)\Delta r)^{3-\gamma} - (j\Delta r)^{3-\gamma}\right] & \text{if } (j+1)\Delta r \leq r_b \\ \frac{1}{3-\beta} r_b^3 \left[\left(\frac{(j+1)\Delta r}{r_b}\right)^{3-\beta} - \left(\frac{j\Delta r}{r_b}\right)^{3-\beta}\right] & \text{if } j\Delta r > r_b. \end{cases} \tag{166}$$

4.2.3   Merger rate for a galactic nucleus

The galactic merger rate is obtained by summing up the rate (157) for each radial shell,

$$\mathcal{R}_{\text{gal}} = \sum_{j \in \mathcal{I}_r} \mathcal{R}_j. \tag{167}$$

4.3 Rate density

The merger rate density $\mathcal{R}_2$ is given by

$$\mathcal{R}_2 = \mathcal{R}_{\text{gal}}\, n_{\text{AGN}}. \tag{168}$$

The average binary merger time τ_{avg} needed for the merger rate density $\mathcal{R}_1$ is obtained by taking the average of all τ_{merger} that are used in $\mathcal{R}_2$.

We adopt estimates for the population parameters from McKernan *et al.* [18]. In the calculations, we will resort to the lower bounds population parameters values and indicate in parenthesis the associated upper limits

⋄ The number N_{BHs} of stellar mass black holes we estimate as 10^4 [10^6]

⋄ The fraction f_b of BH in BH-BH binaries we estimate as 0.01 [0.2]

⋄ The fraction f_d of BH embedded in the disk we estimate as 0.01 [0.7]

⋄ The number density n_{AGN} of active galactic nuclei we estimate as 4×10^4 Gpc^{-3} [3×10^6 Gpc^{-3}]

The remaining parameters we set to canonical values

⋄ $M_{\text{SMBH}} = 1 \times 10^6 M_\odot$

⋄ $\gamma = 1.5$

⋄ $\beta = 3.2$

⋄ $\sigma = 200$ km/s

⋄ $m_{\text{s,max}} = 50000 M_\odot$; $m_{\text{s,min}} = 0.01 M_\odot$; $m_{\text{s,cr}} = 5 M_\odot$

⋄ $m_{\text{BH,max}} = 50 M_\odot$; $m_{\text{BH,min}} = 5 M_\odot$

We use partitions $|\mathcal{I}_r| = 10$ and $|\mathcal{I}_M| = |\mathcal{I}_q| = |\mathcal{I}_{a_0}| = |\mathcal{I}_{e_0}| = 3$. The numerical evaluations of the merger times results in an average binary merger time of $\tau_{\text{avg}} = 6.3 \times 10^6$ years and a galactic merger rate $\mathcal{R}_{\text{gal}} = 0.49$ Gpc^{-3}. We get from the rate formulae (129) and (168)

$$\mathcal{R}_1 \approx 6.3 \times 10^{-3} \text{ year}^{-1} \text{ Gpc}^{-3}, \tag{169}$$

$$\mathcal{R}_2 \approx 1.96 \text{ year}^{-1} \text{ Gpc}^{-3}. \tag{170}$$

We use partitions $|\mathcal{I}_r| = 10$ and $|\mathcal{I}_M| = |\mathcal{I}_q| = |\mathcal{I}_{a_0}| = |\mathcal{I}_{e_0}| = 5$. The numerical evaluations of the merger times results in an average binary merger time of $\tau_{\text{avg}} = 1.1 \times 10^7$ years and a galactic merger rate $\mathcal{R}_{\text{gal}} = 8.69 \times 10^{-5}$ Gpc^{-3}. We get from the rate formulae (129) and (168)

$$\mathcal{R}_1 \approx 3.6 \times 10^{-3} \text{ year}^{-1} \text{ Gpc}^{-3}, \tag{171}$$

$$\mathcal{R}_2 \approx 3.48 \text{ year}^{-1} \text{ Gpc}^{-3}. \tag{172}$$

The rates are not ruled out by LIGO, whose current stellar mass BH binary merger rate is $24 - 112$ year^{-1} Gpc^{-3} [25].

To investigate the effect of eccentric orbits on the merger rate, we perform the same calculation as above but set the initial eccentricity to $e_0 = 1 \times 10^{-3}$ throughout. We obtain an average binary lifetime of $\tau_{\mathrm{avg}} = 2.2 \times 10^8$ years, a galactic rate $\mathcal{R}_{\mathrm{gal}} = 4.3 \times 10^{-6}\,\mathrm{Gpc}^{-3}$ and the associated rate densities

$$\mathcal{R}_1 \approx 1.8 \times 10^{-4} \ \mathrm{year}^{-1}\,\mathrm{Gpc}^{-3}, \tag{173}$$

$$\mathcal{R}_2 \approx 1.7 \times 10^{-5} \ \mathrm{year}^{-1}\,\mathrm{Gpc}^{-3}. \tag{174}$$

This suggests that ignoring eccentricity changes due to binary-disk interaction underestimates the merger rate. Of course, this conclusion is based on a very simplified and idealised binary merger channel. However, one may still conclude that more detailed studies on the binary-disk interaction are needed, especially studies ans simulation with non-zero eccentricities.

References

1. *Stacks Project* https://stacks.math.columbia.edu.

2. Thorne, K. S. Multipole expansions of gravitational radiation. *Rev. Mod. Phys.* **52,** 299–339 (2 1980).

3. Peters, P. C. & Mathews, J. Gravitational Radiation from Point Masses in a Keplerian Orbit. *Phys. Rev.* **131,** 435–440 (1 1963).

4. Peters, P. C. Gravitational Radiation and the Motion of Two Point Masses. *Phys. Rev.* **136,** B1224–B1232 (4B 1964).

5. Hansen, R. O. Post-Newtonian Gravitational Radiation from Point Masses in a Hyperbolic Kepler Orbit. *Phys. Rev. D* **5,** 1021–1023 (4 1972).

6. Turner, M. Gravitational radiation from point-masses in unbound orbits - Newtonian results. *The Astrophysical Journal* **216,** 610–619 (Sept. 1977).

7. Junker, W. & Schaefer, G. Binary systems - Higher order gravitational radiation damping and wave emission. *Monthly Notices of the Royal Astronomical Society* **254,** 146–164 (Jan. 1992).

8. De Vittori, L., Jetzer, P. & Klein, A. Gravitational wave energy spectrum of hyperbolic encounters. *Phys. Rev. D* **86,** 044017 (4 2012).

9. García-Bellido, J. & Nesseris, S. Gravitational wave energy emission and detection rates of Primordial Black Hole hyperbolic encounters. *Physics of the Dark Universe* **21,** 61 –69. ISSN: 2212-6864 (2018).

10. Watson, G. N. *A Treatise on the Theory of Bessel Functions* (Cambridge University Press, 1966).

11. Thompson, T. A., Quataert, E. & Murray, N. Radiation Pressure–supported Starburst Disks and Active Galactic Nucleus Fueling. *The Astrophysical Journal* **630,** 167–185 (2005).

12. Lubow, P. S. H. & Artymowicz. *Evolutionary Processes in Binary Stars* (ed R. A. M. J. Wijers, . C. A. T. M. B. Davies) (NATO ASIC Proc. 477, 1996).

13. Artymowicz, P. & Lubow, S. H. Dynamics of binary-disk interaction. 1: Resonances and disk gap sizes. *The Astrophysical Journal* **421,** 651–667 (Feb. 1994).

14. Hayasaki, K., Mineshige, S. & Sudou, H. Binary Black Hole Accretion Flows in Merged Galactic Nuclei. *Publications of the Astronomical Society of Japan* **59,** 427–441. ISSN: 0004-6264 (2007).

15. Baruteau, C., Cuadra, J. & Lin, D. N. C. BINARIES MIGRATING IN A GASEOUS DISK: WHERE ARE THE GALACTIC CENTER BINARIES? *The Astrophysical Journal* **726,** 28 (2010).

16. Hayasaki, K. A new mechanism for massive binary black hole evolution. *Publ. Astron. Soc. Jpn* **61,** 65 (2009).

17. Goldreich, P. & Sari, R. Eccentricity Evolution for Planets in Gaseous Disks. *The Astrophysical Journal* **585,** 1024–1037 (2003).

18. McKernan, B. *et al.* Constraining Stellar-mass Black Hole Mergers in AGN Disks Detectable with LIGO. *The Astrophysical Journal* **866,** 66 (2018).

19. Kroupa, P. On the variation of the initial mass function. *Monthly Notices of the Royal Astronomical Society* **322,** 231–246 (2001).

20. Lauer, T. R. *et al.* The Centers of Early-Type Galaxies with HST.I.An Observational Survey. *The Astrophysical Journal* **110,** 2622 (Dec. 1995).

21. Schödel, R. *et al.* The distribution of stars around the Milky Way´s central black hole - II. Diffuse light from sub-giants and dwarfs. *A&A* **609,** A27 (2018).

22. A. Rasskazov, B. K. The rate of stellar mass black hole scattering in galactic nuclei. *Submitted to the Astrophysical Journal* (2019).

23. Tout, C. A., Hurley, J. R. & Pols, O. R. Evolution of binary stars and the effect of tides on binary populations. *Monthly Notices of the Royal Astronomical Society* **329,** 897–928. ISSN: 0035-8711 (Feb. 2002).

24. Ablimit, I. & Maeda, K. Monte Carlo Population Synthesis on Massive Star Binaries: Astrophysical Implications for Gravitational-wave Sources. *The Astrophysical Journal* **866,** 151 (2018).

25. The LIGO Scientific Collaboration *et al.* Binary Black Hole Population Properties Inferred from the First and Second Observing Runs of Advanced LIGO and Advanced Virgo. *arXiv e-prints.* arXiv: `1811.12940` `[astro-ph.HE]` (Nov. 2018).

26. Maggiore, M. *Gravitational Waves: Volume 1: Theory and Experiments* (Oxford University Press, 2007).

5 Appendix

5.1 Alternative calculation of frequency spectrum

Equation (65) gives the power emitted in the n-th harmonic of an elliptic Keplerian orbit. Here there is similar derivation of the same result which does not explicitly use Parseval's identity. The calculations follows the textbook by Maggiore [26]. Again, we parametrize an elliptic Keplerian orbit in the form

$$x(\beta) = a(\cos u - e), \tag{175}$$
$$y(\beta) = b \sin u. \tag{176}$$

Here a is the semi-major axis and b is the semi-minor axis of the orbit. The eccentric anomaly u is defined by the Kepler equation

$$u - e \sin u = \omega(t - t_0) \equiv \beta, \tag{177}$$

the time t_0 being an integration constant chosen such that $x(-\beta) = x(\beta)$ and $y(\beta) = -y(-\beta)$. The solution of the Kepler equation can be given as a Fourier expansion involving Bessel functions. To see this we make the Fourier series ansatz

$$y(\beta)\frac{e}{b} = u - \beta = e \sin u = \sum_{n=1}^{\infty} a_n \sin(n\beta), \tag{178}$$

where the coefficients are given by

$$a_m = \frac{2}{\pi} \int_0^\pi d\beta \, (u - \beta) \sin(m\beta). \tag{179}$$

We now compute

$$
\begin{aligned}
a_m &= -\frac{2e}{\pi m} \int_0^\pi d\beta \, \sin u \, \frac{d}{d\beta} \cos(m\beta) \\
&= \frac{2e}{\pi m} \int_0^\pi du \, \frac{d\sin u}{du} \, \cos(m\beta) \\
&= \frac{2e}{\pi m} \int_0^\pi du \, \cos u \, \cos(mu - me \sin u) \\
&= \frac{e}{m} \int_0^\pi \frac{du}{\pi} \, \left[\cos(u(m-1) - me \sin u) + \cos(u(m+1) - me \sin u) \right].
\end{aligned}
$$

By using the following integral representation of the Bessel functions of the first kind

$$J_n(z) = \int_0^\pi \frac{du}{\pi} \cos(nu - z \sin u), \tag{180}$$

we arrive at

$$a_m = \frac{e}{m} \left[J_{m-1}(me) + J_{m+1}(me) \right]. \tag{181}$$

Using the recurrence formula

$$J_{n-1}(z) + J_{n+1}(z) = \frac{2n}{z} J_n(z), \tag{182}$$

43

this result can be rewritten as

$$a_m = \frac{2}{m} J_m(me). \tag{183}$$

Similarly we write $\frac{x(\beta)}{a} = \cos u - e = b_0 + \sum_{n=1}^{\infty} b_n \cos(n\beta)$ and find for the corresponding expansion coefficients

$$b_0 = -\frac{3}{2}e, \tag{184}$$

$$b_m = \frac{1}{m}[J_{m-1}(z) - J_{m+1}(z)] = \frac{2}{m} J'_m(me); \tag{185}$$

the prime denotes the derivative with respect to the argument. Next we compute the Fourier expansion of $x^2(\beta)$, $y^2(\beta)$ and $x(\beta)y(\beta)$. We can again write

$$y^2(\beta) = A_0 + \sum_{n=1}^{\infty} A_n \cos(n\beta), \tag{186}$$

$$x^2(\beta) = B_0 + \sum_{n=1}^{\infty} B_n \cos(n\beta), \tag{187}$$

$$y(\beta)x(\beta) = \sum_{n=1}^{\infty} C_n \sin(n\beta), \tag{188}$$

together with

$$A_m = \frac{2}{\pi} \int_0^{\pi} d\beta \, y^2(\beta) \cos(m\beta), \tag{189}$$

$$B_m = \frac{2}{\pi} \int_0^{\pi} d\beta \, x^2(\beta) \cos(m\beta), \tag{190}$$

$$C_m = \frac{2}{\pi} \int_0^{\pi} d\beta \, x(\beta)y(\beta) \sin(m\beta). \tag{191}$$

Similar to the calculation of a_n we obtain

$$A_m = \frac{b^2}{m} \left[J_{m+2}(me) - J_{m-2}(me) \right],$$

$$B_m = \frac{a^2}{m} \left[J_{m-2}(me) - J_{m+2}(me) - 2e(J_{m-1}(me) - J_{m+1}(me)) \right],$$

$$C_m = \frac{ba}{m} \left[J_{m+2}(me) + J_{m-2}(me) - e(J_{m+1}(me) + J_{m-1}(me)) \right],$$

along with $A_0 = \frac{1}{2}$ and $B_0 = \frac{1+4e^2}{2}$. By the use of the recurrence relations (182) and (185) the above relations can be expressed entirely in terms of J_m and its derivative. We obtain

$$A_m = \frac{4b^2}{me} \left[\frac{1}{me} J_m(me) - J'_m(me) \right],$$

$$B_m = \frac{4a^2}{m} \left[\left(\frac{1}{e} - e \right) J'_m(me) - \frac{1}{me^2} J_m(me) \right], \tag{192}$$

$$C_m = \frac{4ba}{m} \left[\left(\frac{1}{e^2} - 1 \right) J_m(me) - \frac{1}{me} J'_m(me) \right].$$

With the above we are able to expand the second mass moment (23) as

$$\mathcal{G} = \mu \sum_{n=0}^{\infty} \begin{bmatrix} B_n \cos(n\beta) & C_n \sin(n\beta) & 0 \\ C_n \sin(n\beta) & A_n \cos(n\beta) & 0 \\ 0 & 0 & 0 \end{bmatrix} \equiv \sum_{n=0}^{\infty} \mathcal{G}^{(n)}. \tag{193}$$

The emitted power in the quadrupole approximation is obtained from the formulae (18) and (31)

$$P = \frac{8\pi}{75} \sum_{m=-2}^{2} \left\langle \left| {}^{(3)}\mathcal{G}_{a_1 a_2} \left(\mathcal{Y}_{a_1 a_2}^{2m} \right)^* \right|^2 \right\rangle. \tag{194}$$

Since $\langle \cos(n\beta)\cos(m\beta) \rangle = \langle \sin(n\beta)\sin(m\beta) \rangle = \frac{1}{2}\delta_{mn}$, different harmonics don't contribute in the power spectrum. Hence we can set $P = \sum_{n=1}^{\infty} P_n$, where the power radiated in the n-th harmonics is

$$P_n = \frac{8\pi}{75} \sum_{m=-2}^{2} \left\langle \left| {}^{(3)}\mathcal{G}_{a_1 a_2}^{(n)} \left(\mathcal{Y}_{a_1 a_2}^{2m} \right)^* \right|^2 \right\rangle, \tag{195}$$

together with

$$^{(3)}\mathcal{G}^{(n)} = \mu(\omega n)^3 \begin{bmatrix} B_n \sin(n\beta) & -C_n \cos(n\beta) & 0 \\ -C_n \cos(n\beta) & A_n \sin(n\beta) & 0 \\ 0 & 0 & 0 \end{bmatrix}. \tag{196}$$

Using the above formulae gives the power in the n-th harmonic as

$$P_n = \frac{1}{15}\mu^2(\omega n)^6 \left(A_n^2 + B_n^2 + 3C_n^2 - A_n B_n \right). \tag{197}$$

We can now insert the explicit form of the coefficients (192) and after rearranging terms we find that P_n is equal to (65).